Stable bimetallic Ru-Mo/Al$_2$O$_3$ catalysts for the light alkane combustion: Effect of the Mo addition

Katarzyna Adamska[a,*], Janina Okal[a], Włodzimierz Tylus[b]

[a] Institute of Low Temperature and Structure Research, Polish Academy of Sciences, Okólna 2, 52-422 Wrocław, Poland
[b] Department of Advanced Material Technologies, Faculty of Chemistry, Wrocław of University of Science and Technology, Poland

ARTICLE INFO

ABSTRACT

A series of Ru-Mo/γ-Al$_2$O$_3$ catalysts containing fixed Ru loading (5 wt.%) and variable Mo contents (1.6, 4.8 and 9.5 wt.%), were synthesized by co-impregnation method using Ru(NO)(NO$_3$)$_3$ and (NH$_3$)$_6$Mo$_7$O$_{24}$ × 4H$_2$O as metal precursors and their catalytic characteristics were evaluated for the first time in combustion of propane used as a model compound. The effect of the Ru/Mo atomic ratio (3:1, 1:1 and 1:2) on the structure of the reduced samples was investigated by ICP-AES, BET, XRD, HRTEM, SEM-EDX, H$_2$-TPR and chemisorption of hydrogen and oxygen. The surface properties of the catalysts were detailed studied by XPS spectroscopy. Structural characterization data lead to conclusion that a synergy effect of ruthenium and molybdenum is observed in the Ru-Mo/γ-Al$_2$O$_3$ catalysts. An increase of Mo loading caused the formation of smaller nanoparticles (d$_{av}$ = 1.3, 1.0 and 0.8 nm, respectively) as compared to the monometallic Ru system (d$_{av}$ = 1.4 nm). For low Mo loading (Ru:Mo atomic ratio of 3:1) the H$_2$ uptake was higher (H/Ru = 0.55) than in the Ru/γ-Al$_2$O$_3$ sample (H/Ru = 0.52). This leads to the high activity of the 5%Ru-1.6%Mo catalyst in the propane combustion (TOF = 0.034 (s^{-1})). Moreover, the catalytic stability was much higher for the bimetallic Ru-Mo systems than for the monometallic Ru catalyst. Despite their high thermal stability under oxygen-rich atmosphere, bimetallic catalyst containing 4.8%Mo (Ru:Mo atomic ratio of 1:1) was less active in propane oxidation (TOF = 0.016 (s^{-1})) than the Ru system (TOF = 0.029 (s^{-1})). The lower activity results from partial blocking the active centers on the ruthenium by covering them with an inactive MoO$_x$ layer. At the highest Mo content (Ru:Mo atomic ratio of 1:2) the blocking of the active Ru centres increases, much lower H$_2$ chemisorption capacity and a significant increase of the metallic Ru (74%) and metallic Mo (25%) species, resistant to oxidation at low temperature, were observed. This leads to very low activity of the 5%Ru-9.5%Mo catalyst in the propane combustion. Importantly, our studies also revealed that the molybdenum modifies interaction of hydrogen and oxygen with ruthenium in the Ru-Mo catalysts. For hydrogen, the adsorption process becomes activated and Mo species weaken the adsorption strength.

1. Introduction

Volatile organic compounds from car exhaust or industrial processes are the reason of the air pollution and destruction of the Earth's ozone layer. Catalytic combustion of these toxic compounds, including also light hydrocarbons (C1 to C4), is one of the most effective methods of their removal from the waste gases [1]. The volatile hydrocarbons with a low carbon content are considered one of the most difficult to remove, especially at low concentrations. Systems based on noble metals are very active in removing the low-chain hydrocarbons [2], however, they have a number of disadvantages, such as a high cost, limited availability and often unsatisfactory stability. They are partially inactivated at elevated temperatures and are sensitive to poisoning by sulfur,

carbon or chlorine ions [3]. For this reason, heterogeneous catalysts are often modified by the addition of the another metallic component.

Currently, considerable attention is devoted on the catalysis of noble metals (Rh, Ir, Pd, Pt) modified with reducible metal oxide species such as MoO$_x$ or ReO$_x$ [4,5]. The modified bimetallic catalysts may be applied to the various difficult catalytic reactions, for example to the selective hydrogenolysis and selective hydrogenation of carbonyl and carboxyl groups [4,6–8]. Recently, supported ruthenium-modified catalysts, such as Ru-MoO$_x$/SiO$_2$ and Ru-MoO$_x$/C, have been also investigated for the selective hydrogenation of nitroarenes to aminoarenes [9]. Unsupported Ru/Mo catalysts were found as efficient for the selective hydrogenation of a range of amides to the corresponding amines under milder reaction conditions than those reported previously

---

for these difficult transformations and depending on the Mo:Ru atomic ratio, synergistic or poisoning effects were observed [10]. According to our knowledge, the supported bimetallic Ru-Mo nanoparticles have never been used for the propane oxidation. In our previous work we showed that an addition of rhenium to the ruthenium system may improve the activity and stability of the Ru-Re catalysts in the light alkane oxidation [11,12]. However, the price and availability of the molybdenum make this metal much more attractive for the catalytic applications.

Despite the catalytic importance of the Ru-Mo catalysts, the way Ru and Mo interact with each other to have better catalytic properties as compared to the monometallic counterparts, is still not explained. There are many contradictions in Ru-Mo research in the literature. Some reports suggested that addition of Mo to Ru catalyst results in the increase or decrease of Ru dispersion [13], or that the electron transfer from partially reduced MoO_x species to the Ru centers occurs [14], or opposite from the Ru metal species to partially reduced molybdenum species [13]. Successive impregnation or co-impregnation were usually applied as a preparation methods of the supported Ru-Mo catalysts and $RuCl_3$ [13–18] or $Ru_3(CO)_{12}$ [8] were chosen as the Ru precursors, while ammonium heptamolybdate $((NH_4)_6Mo_7O_{24})$ [13–18] or Mo $(CO)_6$ [8] as the Mo precursors. Most of the studies were performed on the Ru-Mo catalysts which were first calcined in air at 400–600 °C and next reduced in H_2 at 300–600 °C [13–17]. The Ru-Mo catalysts without a calcination step were rarely tested [16,17]. However, during the calcination step at high temperature, the formation of the volatile compound RuO_4 must be considered because it can justify a not negligible loss of this metal. Additionally, the negative effect of a calcination step on the mean Ru particle size and catalytic activity was reported for the monometallic Ru catalysts [19,20]. Also, Ru-Mo/SiO_2 catalysts pretreated by the calcination-reduction procedure were less active in CO hydrogenation than those subjected only to the reduction treatment [17]. Furthermore, most of the metal precursors used in the previous studies contain chlorine ligands (from $RuCl_3$ precursor) that might interact with the metal surface causing their contamination. Juan and Damiani [16,17] reported that the presence of residual chlorine in the Ru-Mo/SiO_2 catalysts inhibited both activity and the hydrogen uptake. We also reported large suppression of H_2 chemisorption in the Ru mono- and bimetallic Ru-Re catalysts, prepared from $RuCl_3$ precursor, because of the Ru surface contamination by the Cl species [21,22].

In this report, we have extended previous studies of high-activity alumina supported ruthenium catalysts modified by rhenium [11,12], by probing the effect of modifying of Ru/γ-Al_2O_3 catalysts by molybdenum. It has been shown that Ru-Re/γ-Al_2O_3 catalysts at Re loading of $\leq$ 3 wt.% were more active and stable in the propane combustion than the Ru catalyst [11]. Here, we reported the first data available on the MoO_x modified Ru/γ-Al_2O_3 catalysts for the total oxidation of a short chain alkane. The activity was evaluated for the total oxidation of propane used as a model compound of the short chain alkanes, since light alkanes are emitted from a many range of sources and they are the most difficult VOCs to oxidize. MoO_x modified Ru/γ-Al_2O_3 catalysts were prepared by the co-impregnation method and first it were thoroughly characterized by different techniques, including H_2-TPR, HRTEM, SAED, EDX, XRD, XPS, N_2 adsorption-desorption and H_2 and O_2 chemisorption. The aim of the research was to obtain more information on the impact of the Ru/Mo atomic ratio on the activity and stability of the Ru-Mo/γ-alumina catalysts, as well on the microstructure, ruthenium dispersion, surface properties and interaction between ruthenium and molybdenum in the studied bimetallic systems. To the best of our knowledge, a systematic studies of the impact of molybdenum on the adsorption properties of the Ru-Mo/γ-Al_2O_3 catalysts, especially for hydrogen and oxygen, are very rare. Detailed XPS studies of the Ru-Mo catalysts were also performed since the exact and accurate interpretation of the results obtained has been poorly addressed in the literature. Such studies are very important for

understanding the complex nature of the active centers in the studied Ru-Mo catalysts. In order to avoid poisoning effect of chlorine on the adsorption and catalytic properties of the Ru-Mo/γ-Al_2O_3 catalysts we used $Ru(NO)(NO_3)_3$ as the ruthenium precursor and to date, no studies have been reported on a catalyst preparation starting from this compound. Since Ru-based catalysts are unstable in an oxidizing atmosphere at high temperatures, the prepared Ru-Mo catalysts were subjected to the direct hydrogen reduction treatment.

2. Experimental

2.1. Preparation and treatment of the catalysts

The monometallic (Ru, Mo) and bimetallic Ru-Mo catalysts were prepared by incipient wetness impregnation or co-impregnation methods, respectively. The used alumina support was a high-purity γ-alumina, Puralox from Sasol, which was calcined in air at 550 °C for 20 h before metal precursors were added. After this treatment γ-Al_2O_3 had a BET surface area of 189 m^2/g, a pore volume of 0.50 cm^3/g and an average pore diameter of 7.8 nm. The amount and concentration of the aqueous solutions of metal precursors were adjusted in order to have 5 wt.% Ru and 1.6, 4.8 and 9.5 wt.% of Mo on the final monometallic and bimetallic catalysts (Ru:Mo atomic ratio of 3:1, 1:1 and 1:2, respectively). The high Ru loading was chosen because the observation of the structural changes of the active phase during the procedures used in this work was too difficult in the case of using the less amount of ruthenium. The metal precursors were ruthenium (III) nitrosylnitrate $(Ru(NO)(NO_3)_3$ (Alfa Aesar) and ammonium heptamolybdate $(NH_4)_6Mo_7O_{24} \times 4H_2O$ (POCh, Poland). Impregnated samples were dried overnight in air at 110 °C and then reduced in hydrogen flow (30 cm^3/min) at 500 °C for 4 h (5 °C/min). After cooling to room temperature (RT) in H_2 flow the catalyst samples were slowly exposed to air and stored in a close container before using.

2.2. Catalyst characterization

The Ru and Mo loadings of the reduced catalysts were measured by Inductively Coupled Plasma Atomic Emission Spectroscopy (ICP-AES) with a Thermo Scientific ICAP 7000 equipment. Chemical composition of the prepared samples was checked with a FEI NovaNanoSEM 230 FE-SEM microscope equipped with EDS (EDAX Genesis XM4).

Nitrogen adsorption-desorption isotherms of the reduced samples were obtained at -196 °C using a Micromeritics ASAP 2020 apparatus. The specific surface area (S_{BET}) was calculated using the Brunauer–Emmett–Teller (BET) method. The total pore volume (V_p) was determined at a relative pressure of $P/P_o = 0.99$ while the mean pore diameter (D_p) for mesopores was determined by Barret-Joyner-Halenda (BJH) method from the desorption branch of the isotherm.

Redox behaviour of the catalysts was investigated by the temperature programmed reduction by hydrogen (H_2-TPR) by using a Micrometrics Autochem II 2920 apparatus. The measurements were performed for the catalysts precursors supported on γ-Al_2O_3 i.e., without any previous calcination in air in order to study the interaction between the Ru and Mo species and the support during the reduction process. The TPR analysis was carried out in a reducing mixture (30 cm^3/min) consisting of 5 vol.% H_2 in Ar from RT to 900 °C (5 °C/min). The hydrogen concentration in the effluent stream was monitored by a thermal conductivity detector (TCD).

The crystalline structure of the reduced catalysts was determined by X-ray powder diffraction (XRD) using PANanalytical X'Pert PRO diffractometer with CuKα radiation (λ = 0.15406 nm). Microstructure characterization of the catalysts was examined by high resolution transmission electron microscopy (HRTEM) and selected area electron diffraction (SAED) with Philips CM 20 Super-Twin microscope, which at 200 kV provides a 0.25 nm resolution. In order to determine the particle size distribution, at least 40 TEM images was analysed from

Table 1
ICP-AES measurements of Ru and Mo loadings in the reduced monometallic (Mo, Ru) and bimetallic Ru-Mo/γ-Al$_2$O$_3$ catalysts. EDS analysis and N$_2$ adsorption-desorption results.

Catalyst	Nominal Ru:Mo atomic ratio	Metal loading (wt.%)		EDS analysis Ru:Mo atomic ratio	S_{BET} (m^2/g)	D_p (nm)	V_p (cm^3/g)	Mo surface density[a] (Mo/nm^2)
		Ru	Mo					
γ-Al$_2$O$_3$	–	–	–	–	189	7.8	0.50	–
1.6%Mo/γ-Al$_2$O$_3$	–	–	1.39 ± 0.14	–	191	7.8	0.49	0.53
4.8%Mo/γ-Al$_2$O$_3$	–	–	4.28 ± 0.40	–	192	7.6	0.47	1.55
9.5%Mo/γ-Al$_2$O$_3$	–	–	9.40 ± 0.20	–	182	7.1	0.43	3.28
5%Ru/γ-Al$_2$O$_3$	1:0	4.95 ± 0.09	–	1:0	183	7.8	0.45	–
5%Ru-1.6%Mo/γ-Al$_2$O$_3$	3:1	4.88 ± 0.12	1.41 ± 0.14	4:1	176	7.8	0.45	0.57
5%Ru-4.8%Mo/γ-Al$_2$O$_3$	1:1	5.58 ± 0.40	4.31 ± 0.40	1:0.7	183	7.2	0.42	1.63
5%Ru-9.5%Mo/γ-Al$_2$O$_3$	1:2	4.72 ± 0.40	9.45 ± 1.00	1:1.8	152	7.0	0.34	3.92

[a] Defined as the number of molybdenum atoms per square nanometre of the catalyst.

which the sizes of several hundred metal particles were measured.

The ruthenium dispersion in the catalysts was estimated with the use of a conventional chemisorption technique using hydrogen as the adsorbate. Chemisorption measurements were carried out on the catalyst samples at room temperature and at 100 °C using a standard Pyrex glass volumetric apparatus and procedures given in Ref. [21]. First, the prereduced catalyst sample (~1 g) was *in situ* reduced in H$_2$ at 400 °C for 2 h and next evacuated (10^{-6} Torr) at the same temperature for 2 h. After cooling under vacuum to adsorption temperature, the Pd-membrane-purified hydrogen was introduced and a first isotherm, providing an information about the total hydrogen uptake, was registered in the pressure range of 50–240 Torr. The equilibration time was 1 h for each adsorption point. Next, a second isotherm, taken after 10 min evacuation, which gave an information about an amount of weakly (reversibly) adsorbed hydrogen, was measured. The difference between the total and reversible adsorption yields the amount of strongly (irreversibly) bound hydrogen, which after extrapolation to zero pressure, gave the capacity of a hydrogen monolayer.

Oxygen chemisorption measurements were carried out on the prepared samples at RT and 400 °C using the same volumetric apparatus as for H$_2$ chemisorption. Before the O$_2$ adsorption, about 0.5 g of the catalyst was pretreated in H$_2$ at 400 °C for 2 h and after degassing at the same temperature for 2 h it was cooled to RT under dynamic vacuum. First, the total O$_2$ uptake was measured at RT. Next, the temperature of the sample was raised up to 400 °C under the oxygen atmosphere, kept in isothermal conditions for 1 h, and finally cooled to RT, where the total O$_2$ uptake was measured. These data were used mainly to determine the extent of molybdenum or ruthenium reduction in the mono- and bimetallic catalysts. The oxygen uptake from the bare support was subtracted from the oxygen uptake of the supported catalysts to determine the uptake from the Mo and Ru species. The reproducibility of measurements of the amounts adsorbed both oxygen and hydrogen is better than 0.5 μmol.

X-ray photoelectron spectroscopy (XPS) studies were carried out using a SPECS PHOIBOS-100 hemispherical spectrometer equipped with a Mg source (1253.6 eV) operating at 250 W for high resolution spectra. The analysed surface was of about 8 × 8 mm^2. The surfaces of the reduced and air passivated catalyst samples were analysed in the "as received" form or after Ar$^+$ sputtering in order to reduce the carbon contamination concentration on the surface (1.5 keV, 2 μA/cm^2, 60 s). Spectra were processed and fitted by SPECLAB software using Gaussian-Lorentzian curve profile and Shirley baseline. The spectrometer energy scale was calibrated with Au 4f$_{7/2}$, Ag 3d$_{5/2}$ and Cu 2p$_{3/2}$ lines at 84.2, 367.9, and 932.4 eV, respectively. The binding energy (BE) of Al 2p at 74.64 eV in γ-Al$_2$O$_3$ support was also used as the reference for all spectra. This energy corresponded to 284.8 eV for C 1s contamination carbon estimated for the reduced 9.5% Mo/γ-Al$_2$O$_3$ sample, taken as the reference. The accuracy of the measured binding energies was ± 0.1 eV.

2.3. Catalytic test measurement

The catalytic propane combustion tests were performed using a fixed bed laboratory micro-reactor [11]. The 100 mg of the catalyst pretreated in hydrogen and next in air at 150 °C for 1 h, was loaded in the quartz tube reactor between two layers of quartz beds. The quartz tube was placed in a furnace equipped with a temperature controller. The feed gas contained 800 vppm propane in air with a flow rate of 100 ml min^{-1}. First, the catalyst was activated in the gas mixture for 1 h at 120 °C and next the light-off curve was obtained by increasing the oven temperature by step of 10 °C from 120 to 320 °C. The analyses were made at each temperature until steady-state activity was obtained, and at least two consistent analyses were taken and data averaged. The conversion data were reproducible within 5% accuracy. The concentration of reagents in the gas outlet was determined using a gas chromatograph (Perkin-ElmerARNEL Clarus 500) equipped with thermal conductivity and flame ionization detectors and only CO$_2$ and H$_2$O were detected products indicating that propane was completely oxidized during the progress of the reaction. Specific activity of the catalysts was expressed as turnover frequencies (TOFs). The TOF values were calculated after dividing the oxidation rate expressed in micromoles of propane converted on 1 g of the given catalyst per second (μmol g$_{cat}^{-1}$ s^{-1}) by the active site concentration determined from hydrogen chemisorption data (μmol/g cat.).

3. Results and discussion

3.1. Composition and textural results

Basic characteristics of the reduced monometallic (Mo, Ru) and bimetallic Ru-Mo/γ-Al$_2$O$_3$ catalysts are given in Table 1. The chemical analysis (ICP-AES) results showed that the actual Ru loading in all the catalysts is close to the intended value of 5 wt.%. Also, the Mo loading of Mo/γ-Al$_2$O$_3$ and Ru-Mo/γ-Al$_2$O$_3$ catalysts agree well with the nominal loading of 1.6, 4.8 and 9.5 wt.%, respectively. In the bimetallic samples, the Ru and Mo loadings correspond to the Ru:Mo atomic ratios of 3:1, 1:1 and 1:2, respectively. Composition of the prepared catalysts was also determined by the multi-point EDS analysis (for example see Fig. S1, Supplementary material). The existence of Ru and Mo in bimetallic samples was confirmed (Table 1), and determined Ru:Mo atomic ratios are close to the predicted values. For example, for the 5% Ru-9.5% Mo/γ-Al$_2$O$_3$ catalyst with the predicted 1:2 atomic ratio value, analysis of the EDX spectrum (Fig. S1b) indicates that this sample contain 1.41 atomic% of Ru and 2.56 atomic% of Mo (Ru:Mo = 1:1.8), what is the value within the limits of measurement error. Additionally, only small deviations at various points at the samples were noticed.

The texture data such as specific surface area (S_{BET}), average pore diameter (D_p) and total pore volume (V_p) for all catalysts are listed in Table 1, while the N$_2$ adsorption-desorption isotherms and pore size distributions of the Ru-Mo/γ-Al$_2$O$_3$ catalysts are presented in Fig. S2

(Supplementary material). The textural properties of the γ-Al_2O_3 were not affected by the deposition of small amount of Mo (up to 4.8%) while at the higher molybdenum loading in the Mo and Ru-Mo catalysts slightly lower S_{BET} and V_p compared to the bare support were observed. The S_{BET} of the Mo/γ-Al_2O_3 catalysts ranged from 191 to 182 m^2/g, while the Ru-Mo/γ-Al_2O_3 catalysts from 176 to 152 m^2/g. Only, the 5% Ru-9.5%Mo/γ-Al_2O_3 catalyst has the lowest specific surface area (152 m^2/g) and this result could be partly explained by the pore mouths blocking by a large amount of Mo deposited on the support surface, as suggested by the large drop of total pore volume when going from 5% Ru-1.6%Mo (0.45 cm^3/g) to 5%Ru-9.5%Mo sample (0.34 cm^3/g). All studied catalysts are mesoporous and their mean pore diameter is in the range of 7.8-7.0 nm (Fig. S2, Table 1).

The Mo surface densities calculated from S_{BET} and the Mo loadings are shown in the last column of Table 1. The density corresponding to the monolayer saturation capacity (monolayer surface coverage is defined as the maximum amount of amorphous or two-dimensional metal in contact with the support) on γ-Al_2O_3 has been reported to be 4.6 Mo atoms/nm^2 [23]. As shown in Table 1, the Mo surface densities are in the range of 0.53–3.92 Mo atoms/nm^2 and these values correspond to 11–85% of the monolayer capacity.

3.2. H_2-temperature programmed reduction (TPR)

TPR analysis was carried out for unsupported metal precursors and the samples after impregnation of support with active phase salts and drying at 110 °C. The TPR profiles are shown in Figs. 1 and 2. The reduction profile of unsupported $(NH_4)_6Mo_7O_{24}$ consists of a large peak with a maximum at 770 °C and smaller peak at 806 °C (Fig. 1, *dash* line). The profiles of monometallic Mo/γ-Al_2O_3 catalysts precursors depend on the Mo loading. In the 9.5% Mo/γ-Al_2O_3 sample the hydrogen consumption starts around 330 °C, proceeds with a peak centred at 457 °C and next with a very broad high-temperature peak centred around 843 °C (Fig. 1, profile c). Thus, the alumina supported Mo precursor is much easier to reduce than the bulk $(NH_4)_6Mo_7O_{24}$ crystallites. With decreasing the Mo loading the position of these peaks shift slightly to higher temperatures and the intensity of the peaks decrease (Fig. 1, profiles b and a). However, the reduction of Mo species in the Mo/γ-Al_2O_3 catalysts is not ended even at 900 °C. The low-temperature peaks at 457–502 °C correspond to the reduction of Mo^{6+} to Mo^{4+} in dispersed polymeric Mo structures [24]. The high-temperature peaks in region of 820–900 °C are associated with a further progress in the reduction of the partially reduced Mo species, together with the partial reduction of tetrahedrally coordinated Mo species strongly interacted with γ-Al_2O_3 [24]. The peak temperature for the first reduction decreased with increasing the Mo surface density, suggesting that the reduction of Mo^{6+} to Mo^{4+} is faster in the catalyst sample with the higher Mo loading.
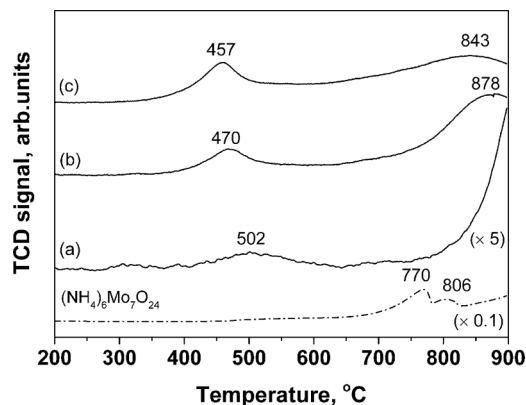
Fig. 2 shows TPR profiles of the $Ru(NO)(NO_3)_3$ precursor, 5% Ru/γ-Al_2O_3 and bimetallic Ru-Mo/γ-Al_2O_3 catalysts precursors in the low-temperature (Fig. 2A) and high-temperature region (Fig. 2B) enlarged 20x in order to show small peaks in details. The reduction profile of $Ru(NO)(NO_3)_3$ shows a large broad peak with a maximum at 221 °C (Fig. 2A, *dash* line). Thus, the reduction of ruthenium salt can be concluded to be completed before reduction of the Mo salt starts (Fig. 1, *dash* line). The TPR profile of the monometallic Ru/γ-Al_2O_3 catalyst shows single narrow reduction peak at lower temperature of 209 °C (Fig. 2A, profile a) and any H_2 consumption in the high-temperature region (Fig. 2B, profile a). The H_2 consumption in the low-temperature region corresponds to the reduction of Ru^{4+} to the $Ru°$ species [22]. For the bimetallic Ru-Mo/γ-Al_2O_3 catalysts shape and position of the reduction peaks of Ru and Mo depend on the Mo loading. The addition of small amount of Mo (Ru:Mo = 3:1) caused the Ru reduction peak slightly smaller and shifted to a higher temperature than in the Ru catalyst (216 °C, Fig. 2A, profile b). The profile shows also the high-temperature very weak broad feature from 480 to 600 °C with maximum at 526 °C (Fig. 2B, profile b) corresponding to the reduction of Mo^{6+} to lower oxidation state species. The reduction profile of the Ru-Mo catalyst with the Ru:Mo = 1:1 consists the broad peak with a maximum similar as for the monometallic Ru catalyst (209 °C) and small peak located at 312 °C (profile c). Interestingly, any appreciable H_2 consumption above 350 °C was not observed (Fig. 2B, profile c). Moreover, Mo reduction peak was at much lower temperature (312 °C) than the 4.8% Mo/γ-Al_2O_3 catalyst (470 °C). The addition of larger amount of Mo to Ru catalyst (Ru:Mo = 1:2) resulted in a change in the peak shape in the low-temperature region and in the shift of the main Ru reduction peak to 228 °C, which can be associated with a small shoulder at lower temperatures (216 °C, Fig. 2A, profile d). In the high-temperature region, the TPR profile contains a very weak reduction feature at around 412 °C and the broad peak at 713 °C (Fig. 2B, profile d). Noticeable shifts in the reduction temperatures of the Ru and Mo components in the bimetallic catalysts can be taken as an evidence of a direct interaction between Ru and Mo species. The existence of an electronic effect cannot be precisely established on the basis of TPR studies. However, it is clearly seen that the presence of Ru enhanced the reduction of MoO_x species. Such a Ru-assisted reduction of MoO_x species likely involves a H_2 dissociation on the formed Ru metallic sites and migration through a spillover mechanism to the neighbouring MoO_x species, promoting their co-reduction [13,14,18].

3.3. Structure characterization

Crystalline phases in the reduced Mo/γ-Al_2O_3, Ru/γ-Al_2O_3 and Ru-Mo/γ-Al_2O_3 catalysts were characterized by X-ray diffraction and XRD patterns are shown in Fig. S3 (Supplementary material) and Fig. 3, respectively. All the reduced samples (Figs. S3 and 3) show diffraction peaks corresponding only to the γ-Al_2O_3 support (JCPDS 29-0063), indicating that these catalysts contained very small crystallites (< 2–3 nm) or the active phase is amorphous or two-dimensional. The absence of any crystalline Mo species is not unexpected since the estimated Mo surface density (Table 1) is below monolayer capacity [23].

Fig. 4 shows representative HRTEM images and SAED patterns of the reduced monometallic Mo/γ-Al_2O_3 catalysts. It is quite difficult to detect molybdenum in TEM images of a low-loaded Mo catalyst (Fig. 4A). However, for the samples of the 4.8% Mo and 9.5% Mo catalysts very small particles with size ≤ 1 nm, possibly connected with the Mo phase, could be found (Fig. 4B and C). The concentration of small particles increase with increasing of the Mo loading. In the SAED patterns (*insets* in Fig. 4A and C) only broad rings of γ-Al_2O_3 are visible. Therefore, identification of the small particles cannot be done by HRTEM or SAED since they are too small to exhibit lattice fringes or visible diffraction features. Since molybdenum in the Mo/γ-Al_2O_3 catalysts is hardly reducible (Fig. 1) we suppose that at low loadings a prevalence of isolated MoO_x species occurs while at higher Mo loadings
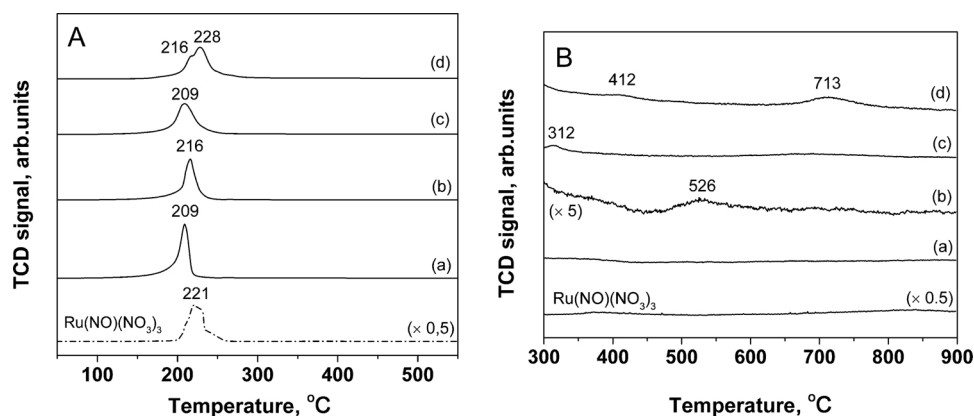

Fig. 1. TPR profiles of $(NH_4)_6Mo_7O_{24}$ precursor (*dash* line) and Mo/γ-Al_2O_3 catalysts with 1.6%Mo (a), 4.8%Mo (b) and 9.5%Mo (c).

Fig. 2. TPR profiles of Ru(NO)(NO$_3$)$_3$ precursor (*dash* line), 5%Ru/γ-Al$_2$O$_3$ (a) and bimetallic Ru-Mo/γ-Al$_2$O$_3$ catalysts containing 1.6%Mo (b), 4.8%Mo (c) and 9.5% Mo (d). Low temperature region (A) and high temperature region enlarged 20 times (B).
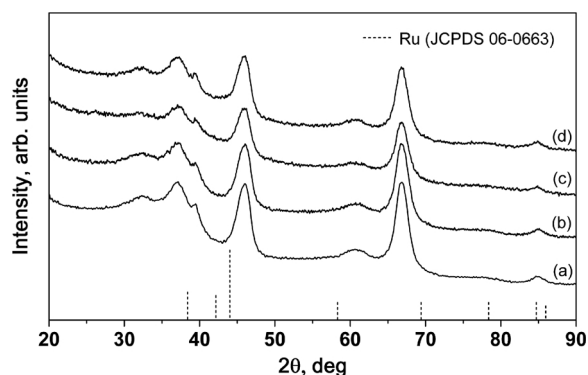

Fig. 3. X-ray diffraction patterns of the 5%Ru/γ-Al$_2$O$_3$ (a) and bimetallic Ru-Mo/γ-Al$_2$O$_3$ catalysts with the loading of 1.6%Mo (b), 4.8%Mo (c) and 9.5%Mo (d). JCPDS data for Ru (File No. 06-0663) is also shown. All visible diffraction peaks correspond only to γ-alumina (JCPDS 29-0063).

occurrence of associated/polymeric (MoO$_x$)$_n$ species is also possible [25].

Representative HRTEM images, SAED patterns (included as an insets) and particle size distributions of the bimetallic Ru-Mo and monometallic Ru/γ-Al$_2$O$_3$ catalyst are shown in Fig. 5 and Supplementary material), respectively. The HRTEM measurements in Fig. S4 (presented in our earlier study [22]) indicate the Ru particle sizes in range of 0.6 to 4.5 nm, with mean size of 1.4 nm. HRTEM images of the bimetallic Ru-Mo/γ-Al$_2$O$_3$ catalysts also contain highly dispersed particles uniformly distributed on the support (Fig. 5). The mean particle size of 1.3 nm obtained for the sample with small amount of Mo (1.6 wt. %) is similar to that in the monometallic Ru sample. With rise of the Mo loading considerable percentage increase of the particles with diameter equal or below 1–1.5 nm occurs and the mean particle size decreases to 1.0 nm for the 5%Ru-4.8%Mo and to 0.8 nm for the 5%Ru-9.5%Mo catalysts (Fig. 5B, C). The metal particles in all bimetallic Ru-Mo catalysts were also too small to exhibit lattice fringes or visible diffraction features and thus SAED patterns contain only rings ascribed to the support structure (inset to Fig. 5A). Yang et al. [18] also found by HRTEM that 5%Ru-10%MoO$_x$/C catalyst showed better dispersion as compared to the monometallic Ru catalyst, by observing the smaller average particle size (1.8 nm) as compared to the 5% Ru/C catalyst (2.6 nm). According to these authors the MoO$_x$ species was in close contact with the Ru moiety in the Ru-Mo/C catalyst, which induces the electron transferring from MoO$_x$ to Ru and this result was well consistent with their XPS measurement [18].

3.4. XPS studies

The XPS technique was used to establish the composition and the oxidation states of the surface molybdenum and ruthenium atoms in the reduced monometallic (Mo, Ru) and bimetallic Ru-Mo/γ-Al$_2$O$_3$ catalysts as well as to verify the interaction between Ru and Mo species. The XPS results were analysed in the binding energy (BE) regions of Mo 3d, Ru 3d, Ru 3p, Al 2p, O 1 s and C 1 s A spectroscopic grade crystalline MoO$_3$ powder (Johnson & Matthey) and 9.5% Mo/γ-Al$_2$O$_3$ catalyst calcined in air at 500 °C for 5 h were analysed as reference materials.

3.4.1. Identification of the Mo oxidation states in the mono-and bimetallic Ru-Mo samples

Molybdenum in bulk oxides and Mo-containing catalysts may have a wide range of oxidation states ranging from $+2$ to $+6$. The literature data indicate that the Mo 3d$_{5/2}$ peak binding energies corresponding to the oxidation states of Mo (VI), Mo (V), Mo (IV) and Mo(0) are at 232.5–232.8 eV [26–28], 231.6 eV [29,30], 229.1–229.3 eV [26,31] and 228.3-228.1 eV [26,32], respectively. The supported Mo-containing catalysts both monometallic [24,28] and bimetallic such as Pt-Mo or Pd-Mo have been extensively analysed by XPS [5,33,34]. Also, unsupported Ru-Mo [10] and supported Ru-Mo catalysts [18] have been recently studied by XPS. The exact and accurate interpretation of the results obtained, however, has been poorly addressed in the literature since the complexity of the XPS spectra. The problem involved in the correct interpretation of XPS spectra of molybdenum oxides is illustrated, for example, by the case of MoO$_2$, for which Mo(IV) in MoO$_2$ spectrum is modelled using a single pair of doublet peaks or two doublets [26]. A degree of complexity is added if other oxidation states are involved, such as the presence of Mo(VI) or Mo(V) [35]. Additionally, supported Mo oxide may be slightly reduced under x-ray irradiation during extended XPS data acquisition [36].

In the bimetallic Ru-Mo and Mo catalysts the molybdenum species can exists at various oxidation states, including also Mo(0). Since Argon sputtering could reduce Mo oxides to mixture of lower oxidation states, therefore we first conducted two independent series of studies in which the surfaces of the MoO$_3$ oxide and the 9.5% MoO$_3$/γ-Al$_2$O$_3$ catalyst were bombarded with Ar$^+$ beam at different times and different beam energy. As a result, Mo 3d spectra were obtained from a single Mo(VI) component, by sequentially photo-reduced Mo(V) and Mo(IV) unscreened and screened, which allowed the respective oxide energy values to be assigned to the oxides (Table 2). Figs. S5 and S6 (supplementary materials) show XPS core level Mo 3d spectra of the crystalline MoO$_3$ oxide and the calcined 9.5% MoO$_3$/γ-Al$_2$O$_3$ catalyst, respectively. The detailed curve fitting procedure is also described in the Supplementary materials.

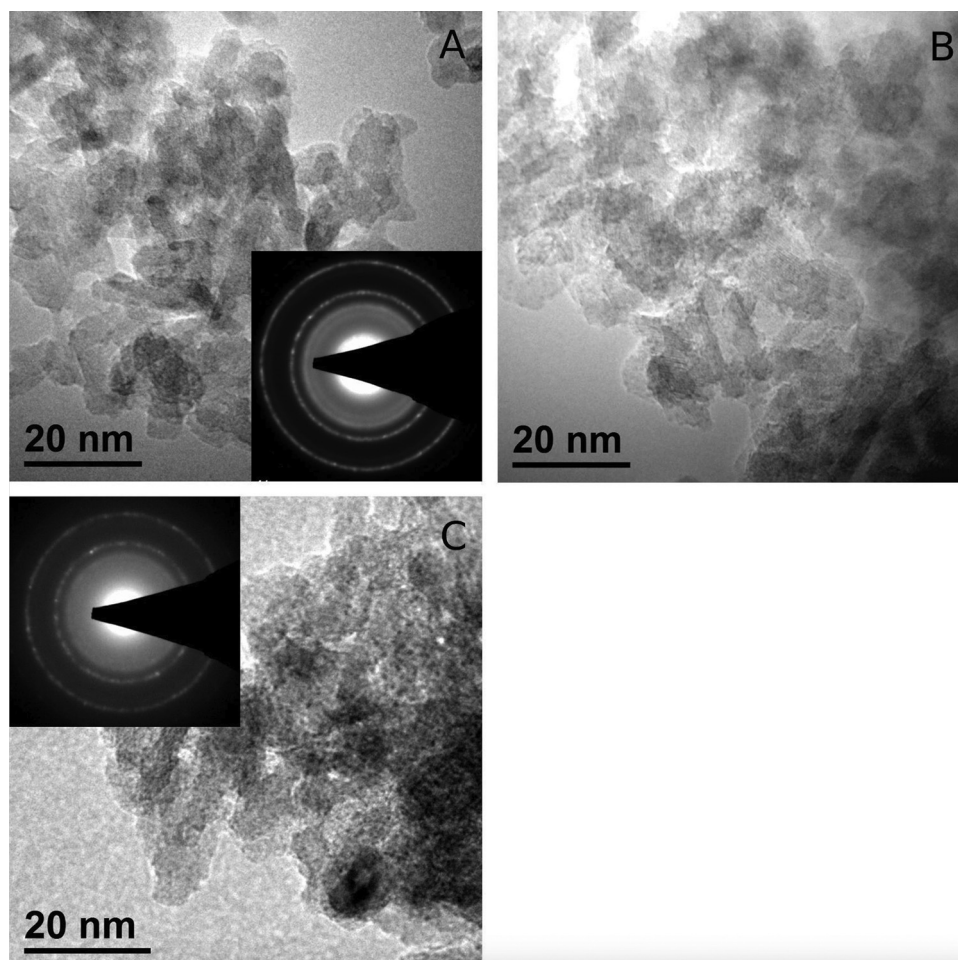The molybdenum oxide binding energies shown in Table 2, were

Fig. 4. Representative HRTEM images and SAED patterns (*insets*) of the reduced monometallic Mo/γ-Al$_2$O$_3$ catalysts with the loading of 1.6%Mo (A), 4.8%Mo (B) and 9.5%Mo (C).

used to establish the oxidation states of the surface molybdenum atoms in the reduced Mo/γ-Al$_2$O$_3$ and Ru-Mo/γ-Al$_2$O$_3$ catalysts. We utilize also observation that Mo(VI) species, highly dispersed on γ-alumina, were reduced very slowly (mainly to Mo^{5+}) during low beam energy Ar$^+$ sputtering. Therefore, we decided to include in Table 3 and in Figs. 6 and 7, the results of surface analysis of the reduced catalysts after cleaning by Ar$^+$ sputtering for 60 s with a low beam energy (1.5 keV, 2 μA/cm^2). The additional justification for this approach was that before the samples were placed in the UHV chamber, they had a brief exposure to atmospheric air, resulting in a carbon contamination and by the way, partially re-oxidized. It was found that the re-oxidation of Mo species was the higher the more surface was originally reduced.

Fig. 6 shows XPS high resolution spectra of Mo 3d with their de-convolution for the Mo/γ-Al$_2$O$_3$ catalysts (left site) and bimetallic Ru-Mo/γ-Al$_2$O$_3$ catalysts (right site) reduced at 500 °C. Table 3 summarizes curve-fitting results obtained for these samples. Spectra of the Mo/γ-Al$_2$O$_3$ and Ru-Mo/γ-Al$_2$O$_3$ catalysts have peaks ascribed to Mo^{6+} species (BE of Mo 3d$_{5/2}$ at 233.2 eV) and additional low-binding components which can be related to lower Mo oxidation states (Mo^{5+} and Mo^{4+}) and also to Mo in the metallic state (Mo 3d$_{5/2}$ at 228.1 eV). The intensity of the peaks ascribed to Mo^{6+} species decreases with the increase of the Mo loadings both in the mono- and bimetallic samples. In the low loaded Mo/γ-Al$_2$O$_3$ catalysts (1.6 and 4.8% Mo) only Mo^{6+}, Mo^{5+} and Mo^{4+} species are detected, but at the high Mo loading (9.5 wt.%) the metallic Mo(0) species are also present (4.3%, Table 3). The calculated average oxidation state of molybdenum in the Mo/γ-Al$_2$O$_3$ catalysts decreases from 5.4 to 4.7 when the Mo loading increases from 1.6 to 9.5%. In the bimetallic Ru-Mo catalysts, the reduction of

MoO$_x$ species is clearly enhanced by the presence of metallic ruthenium and significantly depends on the Ru:Mo atomic ratio. At the Ru:Mo ratio of 3:1 (1.6% Mo loading) the average oxidation state of Mo amounts to 5.1 and decreases to 3.7 at the Ru:Mo ratio of 1:2 (9.5% Mo loading). The lower average oxidation state of Mo results mainly from larger amount of the metallic Mo in the bimetallic Ru-Mo samples, especially for that containing the high Mo loading. On the surface of the 5%Ru-9.5%Mo catalyst, the contribution of Mo(0):Mo(total) equals to about 25%, while on the surface of the monometallic 9.5% Mo catalyst only to 4% (Table 3). In the bimetallic Ru-Mo samples containing 4.8 and 1.6 wt.% of Mo, only 8 or 5.2% molybdenum oxide species is reduced to the metallic form, respectively, whereas in the Mo/γ-Al$_2$O$_3$ catalysts with the same Mo loading, Mo(0) was not detected (Table 3). The XPS results are more detailed than the TPR data and clearly show that reduction process of the bimetallic Ru-Mo catalysts proceeds through the sequence Mo^{6+} → Mo^{5+} → Mo^{4+} → Mo°. These results confirm a promoting role of Ru in the molybdenum reduction process. Evidently, the activation of hydrogen by the metallic ruthenium facilitate molybdenum reduction to lower oxidation states. Interestingly, Beamson et al. [10] found by XPS that the unsupported Ru/Mo catalysts contained also four distinct components with Mo 3d$_{5/2}$ lines centred at 232.4, 231.3, 228.7 and 228.0 eV which were assigned to the Mo^{6+}, Mo^{5+}, Mo^{4+} and Mo° species, respectively. It can be noted that Mo 3d peaks obtained from the reduced Mo/γ-Al$_2$O$_3$ catalysts are much broader (FWHM = 3.46 - 3.27 eV) than those from the Ru-Mo/γ-Al$_2$O$_3$ catalysts (FWHM = 2.84–2.97 eV, Fig. 6).
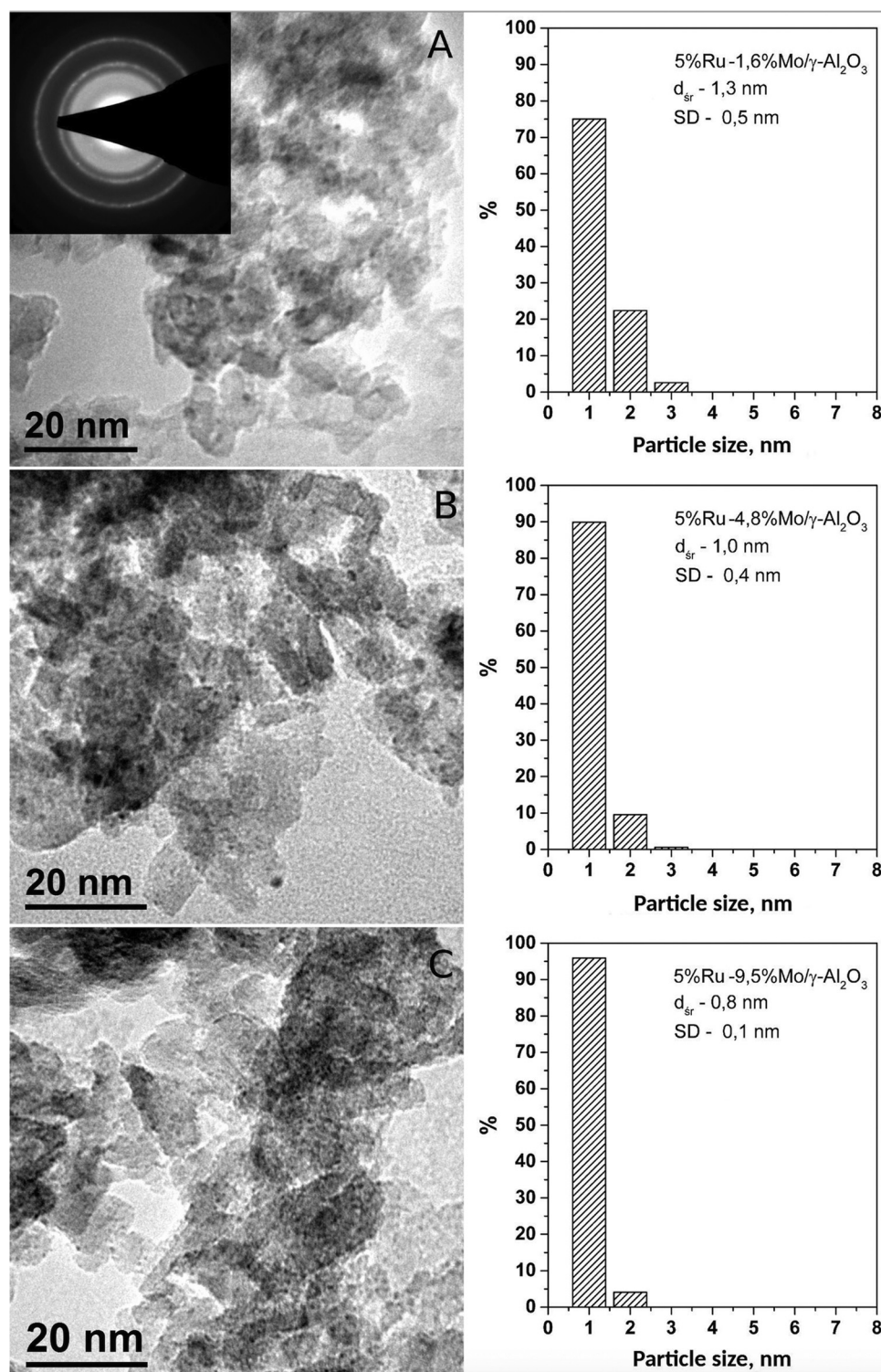
Fig. 5. Representative HRTEM images, SAED patterns (*insets*) and corresponding particle size distribution of the bimetallic 5%Ru-Mo/γ-Al₂O₃ catalysts with the Mo loading of 1.6% (A), 4.8% (B) and 9.5% (C).

3.4.2. Identification of the Ru oxidation states in the bimetallic Ru-Mo samples

Fig. 7 shows the XPS high resolution spectra of the Ru 3d region for the bimetallic Ru-Mo/γ-Al₂O₃ catalysts (traces a–c). The characterization of Ru oxidation states by XPS is complicated by the overlapping of the Ru $3d_{3/2}$ peak with the C 1 s peak at 284.8 eV. The decomposition of the Ru 3d and C 1 s profiles was made subject to the constrains of the constant Ru 3d doublet separation (4.17 eV) and the constant Ru $3d_{5/2}$/

Ru $3d_{3/2}$ intensity ratio equal to 3:2. The deconvolution of Ru 3d – C 1 s spectra was based on the model presented in our previous works [11,37,38]. As shown in Fig. 7, all the Ru 3d spectra exhibit peaks at 280.15 eV and 284.32 eV assigned to the metallic ruthenium [11,37] and peaks centred at 281.10 and 285.27 eV, which are assigned to the oxidized Ru⁴⁺ species, as well as additional weaker peaks at 282.90 and 287.07 eV. These peaks have been identified as a characteristic satellite feature in RuO₂ probably due to unscreened final state effect

Table 2

Binding energy (BE) values (eV) of crystalline MoO_3 generated by Ar^+ sputtering process.

Mo(VI)		Mo(V)		Mo(IV) unscreened		Mo(IV) screened		Mo(0)[a]	
$3d_{5/2}$	$3d_{3/2}$	$3d_{5/2}$	$3d_{3/2}$	$3d_{5/2}$	$3d_{3/2}$	$3d_{5/2}$	$3d_{3/2}$	$3d_{5/2}$	$3d_{3/2}$
233.15	236.30	232.00	235.15	231.05	234.20	229.80	232.94	228.10	231.25
233.10[b]	236.23[b]								
(1.29)[c]	(1.29)	(1.29)	(1.29)	(1.29)	(1.29)	(1.49)	(1.49)	(1.34)	(1.34)

[a] BE for Mo(0) estimated in separate experiment/test.

[b] BE for Mo(VI) in amorphous 9.5% MoO_3/γ-Al_2O_3.

[c] Full width of half maximum (FWHM), eV.

Table 3

Distribution of the oxidation states of surface Ru and Mo atoms and atomic ratios of Ru/Mo, Ru/Al and Mo/Al calculated on the basis of the XPS spectroscopy analysis of the Mo/γ-Al_2O_3, Ru/γ-Al_2O_3 and bimetallic 5% Ru - x% Mo/γ-Al_2O_3 catalysts reduced at 500 °C.

Catalyst	Ru $3d_{5/2}$[a]		Mo $3d_{5/2}$[a]				Atomic ratio					
	Ru^o	Ru^{4+}	Mo^o	Mo^{4+}	Mo^{5+}	Mo^{6+}	Ru/Mo		Ru/Al		Mo/Al	
							XPS	Bulk[b]	XPS	Bulk[b]	XPS	Bulk[b]
1.6%Mo			–	20.8	21.4	57.8					0.006	0.009
4.8%Mo			–	30.0	24.7	45.3					0.024	0.027
9.5%Mo			4.3	36.2	28.2	31.3					0.054	0.056
5%Ru	28.0	72.0	–	–	–	–	–	–	0.10	0.026	–	–
Ru-1.6%Mo	18.8	81.2	5.2	17.7	23.3	58.8	4.7	3.0	0.10	0.027	0.013	0.010
Ru-4.8%Mo	52.2	47.8	8.0	17.4	28.0	46.6	2.2	1.0	0.19	0.028	0.087	0.028
Ru-9.5%Mo	73.8	26.2	24.6	27.8	24.0	23.5	1.2	0.5	0.22	0.030	0.177	0.058

[a] Concentration (atomic %) of Ru $3d_{5/2}$ and Mo $3d_{5/2}$, respectively.

[b] The bulk atomic ratio calculated from the overall chemical composition of the given catalyst.

[39]. The XPS spectrum of the 5% Ru/γ-Al_2O_3 catalyst for the Ru 3d level is very similar to the spectrum of the bimetallic 5% Ru-1.6%Mo/γ-Al_2O_3 catalyst (Fig. 7, trace a) and that reported earlier [37], so it is not presented. It can be noticed that the bimetallic 5%Ru-1.6% Mo (Fig. 7, trace a) and 5% Ru catalyst have more intensive peaks assigned to the oxidized Ru species as compared to the samples with higher Mo loadings (Fig. 7, traces b and c). Previously we found by XPS and O_2 adsorption studies that highly dispersed Ru particles in the Ru/γ-Al_2O_3 catalyst were easily oxidized even at room temperature [11,37,38]. Thus, the presence of the Ru^{4+} species on the surface of bimetallic Ru-Mo catalysts can be partly associated with re-oxidation of the Ru metal species during the transfer to the XPS UHV. On the other hand, however, with the rise of the Mo loading in the Ru-Mo samples more intense contributions from metallic Ru (280.15 eV) were detected and simultaneously the contributions from Ru^{4+} species (281.10 eV) were much less (Fig. 7), indicating that an intensive Ru oxidation is hampered during short exposition to the contact with the atmospheric air. Data of Table 3 show that in the Ru-1.6%Mo sample only 18.8% of ruthenium is in the metallic state while in the catalysts containing 4.8 or 9.5% Mo, the amount of metallic Ru is much higher, 52.2% and 73.8%, respectively. In the monometallic 5% Ru/γ-Al_2O_3 catalyst about 28% of ruthenium remains in the metallic state. The differences in the amount of Ru metal in the 5% Ru sample and 5% Ru-1.6% Mo are caused by higher dispersion of the bimetallic sample. Importantly, analysis of the Ru 3p region (spectra not shown) verified also the presence of metallic Ru (Ru $3p_{3/2}$ at 461.3 eV) and Ru^{4+} species (462.7 eV) as well as increase of metallic Ru species with the rise of Mo loading in the bimetallic catalysts. Interestingly, when the most of Ru is in the metallic form, as stated for the 5%Ru-9.5% Mo catalyst, it is conductive to maintaining larger amount of Mo in the metallic form as well (~25%, Table 3). The XPS results may be interpreted also as a synergistic interaction between the metals in the sense that Ru seems to promote the reduction of Mo, whereas Mo inhibits the oxidation of Ru and this effect is related to the amount of Mo added to the Ru catalyst (Table 3). Therefore, XPS studies evidenced that the increase of Mo loading cause

that more of metallic Ru and metallic Mo phase exists on the surface of the bimetallic samples and these species are probably covered by the very thin layer of oxidized molybdenum species which prevented oxidation of both metallic Ru and Mo. Electronic modification of Ru atoms by Mo atoms, which may also inhibits the Ru oxidation, is rather unlikely since the binding energy of $3d_{5/2}$ Ru electrons (280.15 eV) is independent from the catalyst composition, indicating that if any electronic modification of Ru occurs, it is very slight.

Table 3 summarizes curve-fitting results determined for the monometallic (Mo, Ru) and bimetallic Ru-Mo catalysts. For the Mo/γ-Al_2O_3 catalysts the concentration of Mo^{6+} species decreases monotonically with Mo loading and simultaneously concentration of Mo^{5+} and Mo^{4+} species increase. Sample with the highest Mo loading shows the highest proportion of Mo^{4+} species (36%), with the remainder present as Mo^{5+} (28%) and Mo^{6+} species (31%). For the Ru-Mo/γ-Al_2O_3 catalysts the increase of Mo loading from 1.6 to 9.5% cause that the proportion of Mo^{4+} species ranges from 18% to 28%, Mo^{5+} from 23% to 24% and Mo^{6+} from 59% to 23% (Table 3). The substantial loss of Mo^{6+} for the 5% Ru-9.5% Mo sample seems to be related to the formation of larger amount of metallic Mo° species (25%).

The XPS determined Ru/Mo atomic ratios for the bimetallic catalysts are higher than the bulk atomic ratios, calculated from the overall chemical composition of these samples (Table 3). Moreover, the much larger surface (Mo/Al)$_{XPS}$ atomic ratios of the bimetallic Ru-Mo catalysts compared to monometallic Mo catalysts indicated a larger Mo species surface exposure in the former samples. Fig. S7 (Supplementary Materials) shows the (Mo/Al)$_{XPS}$ ratio of the Mo and Ru-Mo catalysts as a function of nominal Mo/Al ratio. For the monometallic Mo catalysts the concentration of surface dispersed Mo species is very close to the nominal Mo/Al atomic ratio (i.e., (Mo/Al)$_{bulk}$), so we may assume that the whole amount of Mo is probed by XPS. Additionally, the results of Fig. S5 and Table 3 show that at the same Mo loading, the surface coverage of Mo species in the bimetallic Ru-Mo catalysts (except of the low-loaded Mo sample) is much higher than in the Mo/γ-Al_2O_3 samples and also higher than that in the bulk. XPS is very surface sensitive
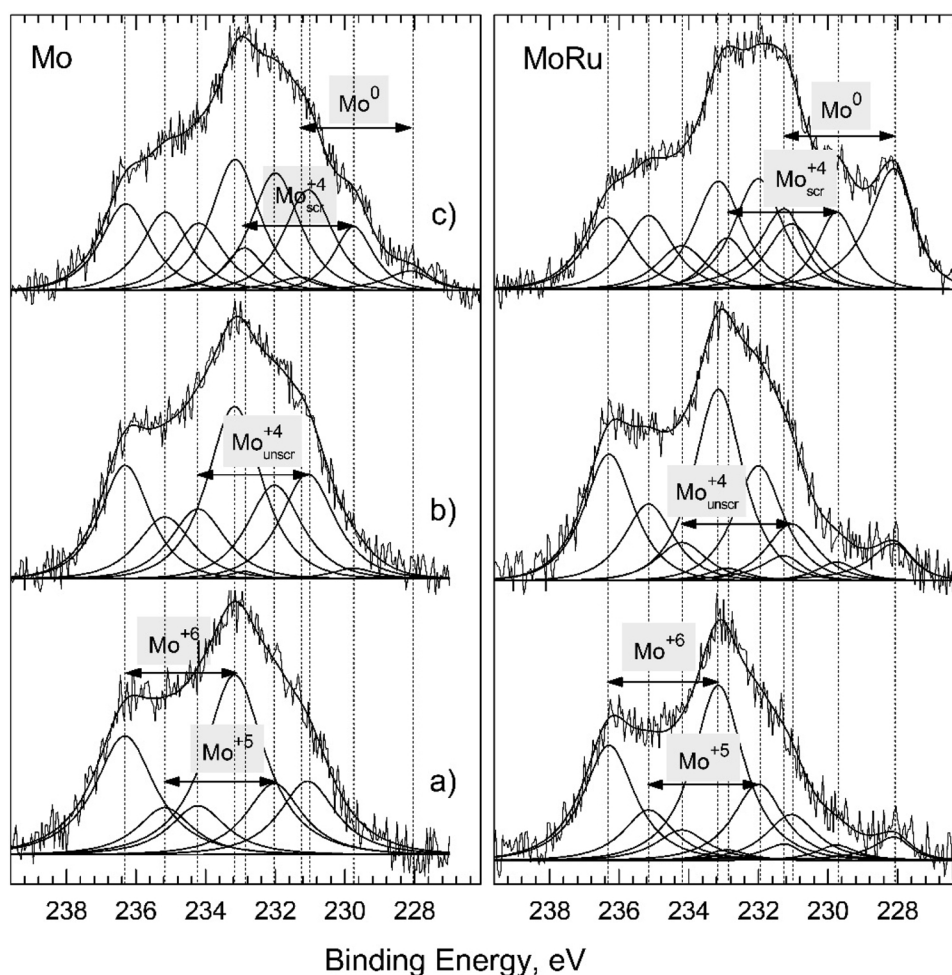
Fig. 6. XPS Mo 3d core level spectra of reduced Mo/γ-Al$_2$O$_3$ (left side) and Ru-Mo/γ-Al$_2$O$_3$ (right side) catalysts containing a) 1.6%Mo, b) 4.8%Mo and c) 9.5%Mo obtained after Ar$^+$ low beam energy cleaning (1.5 keV, 2 μA/cm^2, 60 s).

technique and for this technique it is assumed that maximum sampling depth not exceed the value of $3\lambda_x^y$ (where λ_x^y denotes the Inelastic Mean Free Pathway of x-photoelectron in y solid) but 2/3 of the photoelectrons included in the peak are originate only from 1λ (for molybdenum: λ_{Mo3d}^{MoO3} = 2.0 nm and λ_{Mo3d}^{Mo} = 1.7 nm, [40]). On the basis of these calculations, we can estimate that 2/3 of the Mo particles have sizes below 2 nm and this result is in full agreement with HRTEM studies (Fig. 5). Moreover, this large increase of the surface Mo enrichment indicate that the molybdenum is redispersed and nearly all Mo species are located at the surface of the bimetallic catalysts. Also, the Ru/Al surface ratio is much higher than that in the bulk and increase with Mo loading in the Ru-Mo catalysts (Table 3). This suggests that ruthenium is highly dispersed and located mainly on the outer surface of the support. However, surface enrichment by Ru is not related to the hydrogen chemisorption inhibition on the Ru-Mo catalysts (see *3.6. Chemisorption of hydrogen*).

Concluding, XPS results might suggest that increase of the Mo loading in Ru-Mo/γ-Al$_2$O$_3$ systems magnified the redistribution and migration of MoO$_x$ species to decorate the surface Ru species due to the close contact between Ru and Mo, in full agreement with previous literature data in the other metal/metal oxide systems such as Rh-Mo/SiO$_2$ [6] or Pt-Mo/SiO$_2$ [33]. Moreover, for all bimetallic Ru-Mo/γ-Al$_2$O$_3$ catalysts, enriching the catalyst surface with active phase particles determined by XPS is in line with HRTEM data (Fig. 5). Boufaden et al. [33] found by XPS and HRTEM that larger Mo loadings (12 and 15 wt.%) in the Pt-Mo/SiO$_2$ catalysts induced the formation of MoO$_x$-Pt core-shell nanoparticles which was the reason for the decrease of their

activity. In our case, the formation of MoO$_x$–RuMo core-shell bimetallic nanoparticles is not confirmed by XPS although a significant increase of metallic Ru (74%) and Mo (25%) species resistant to oxidation (Table 3) was observed in the 5%Ru-9.5%Mo catalyst for which the mean size of particles was very small (0.8 nm, Fig. 5). Highly dispersed Ru phase is very prone to oxidation even at RT, therefore it is very likely that in the bimetallic Ru-Mo catalysts the metallic Ru and Mo species are protected against oxidation by the thin layer of MoO$_x$ species.

3.5. Oxygen chemisorption experiments

Verification of the XPS results was done by independent technique, e.g. an oxygen consumption during a reoxidation of the studied catalysts. Desican et al. [41] based on the oxygen chemisorption at high temperature suggested that reduction and reoxidation at 400 °C were appropriate procedure for titrating surface molybdenum atoms in the Mo/alumina catalyst. Leclercq et al. [34] also showed that the amount of oxygen consumed during the oxidation of the Pt-Mo/SiO$_2$ catalysts at 300 °C may be used to calculate the average oxidation state of Mo in the reduced samples. In this study, oxygen chemisorption experiments were performed at RT and 400 °C over all studied catalysts after their *in situ* reduction in adsorption apparatus and the results are presented in Table 4. On the Mo/γ-Al$_2$O$_3$ catalysts only small amounts of O$_2$ were adsorbed at RT. At 400 °C, oxygen adsorption is much higher and increases with the Mo loading. The average oxidation state of Mo calculated from these data decreases monotonically from 5.30 to 5.16 and to 4.78 for the Mo/γ-Al$_2$O$_3$ catalysts containing 1.6%, 4.8% and 9.5%
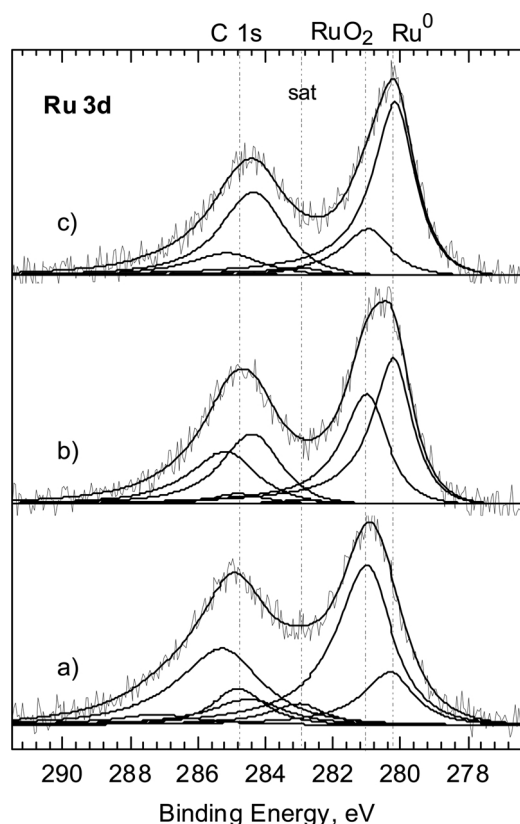
Fig. 7. XPS Ru 3d core level spectra of reduced Ru-Mo/γ-Al$_2$O$_3$ catalysts containing a) 1.6%Mo, b) 4.8%Mo and c) 9.5%Mo obtained after Ar$^+$ low beam energy cleaning (1.5 keV, 2 μA/cm^2, 60 s). Spectra obtained after Ar$^+$ low beam energy cleaning (1.5 keV, 2 μA/cm^2, 60 s).

Mo, respectively. These values are very close to that determined from XPS (Table 4, last column), confirming a validity of the assumptions and calculation method used in the XPS analyses.

The oxygen chemisorption results for highly dispersed 5% Ru/γ-Al$_2$O$_3$ catalyst show that at RT most of the metallic Ru species (90%) was oxidized to RuO$_2$. The O$_2$ uptake value at 400 °C was slightly higher than the theoretical value needed for the total oxidation of Ru to RuO$_2$ (571.6 μmol/g cat. instead of 495 μmol/g cat.) suggesting the formation of some amount of RuO$_4$ oxide and/or additional oxygen adsorption on the RuO$_2$ surface [11,42]. The oxygen uptakes on the bimetallic Ru-Mo/γ-Al$_2$O$_3$ catalysts are higher both at RT and 400 °C and they increase with the Mo loading (Table 4). Additionally, the O$_2$ adsorption at RT on the bimetallic catalysts is higher by 6% to 45% than the sum of the values for the monometallic (Mo, Ru) samples. At temperature of 400 °C, the O$_2$ uptakes for the Ru-Mo catalysts containing 1.6% and

4.8% of Mo are similar or only slightly higher than the sum of the values for the monometallic Ru and Mo catalysts measured at the same temperature. Accordingly, the average oxidation state of Mo is only a bit lower than in the corresponding reduced Mo samples and it is very close to that calculated from XPS data (Table 4). However, for the 5% Ru-9.5%Mo/γ-Al$_2$O$_3$ catalyst (Ru:Mo = 1:2), the O$_2$ adsorption at 400 °C is much higher (by ~59%) than the sum of the O$_2$ uptakes for the monometallic (Mo, Ru) catalysts. The calculated average oxidation state of Mo in this sample is close to +2 and it is much lower than in the bimetallic samples with the lower Mo loadings (~+5, Table 4). Moreover, some contradiction occurs between the average oxidation state of Mo estimated from the oxygen adsorption (+2) and XPS analysis (+3.7). Probably, in the reduced Mo-rich bimetallic catalyst, much more of the molybdenum species is in the close contact with the Ru atoms causing their easier reduction to the metal state (Mo°) or to lower oxidation states than in the catalysts with lower Mo loading. The 5%Ru-9.5%Mo catalyst is characterized by the high oxygen consumption even at RT (793.3 μmol/g, Table 4). This result may indicate that a large amount of highly reduced Mo species is at the nanoparticle surface and thus they are easily susceptible to the oxidation process. This phenomenon may explain some disagreement of the XPS results (*ex-situ* characterization after air exposition at RT) and oxygen adsorption results (*in-situ* characterization).

3.6. Chemisorption of hydrogen

The hydrogen chemisorption has been rarely used for characterization of the bimetallic Ru-Mo catalysts [15–17]. Scott et al. [15] determined the Ru dispersion in the Ru-Mo/ZrO$_2$ catalysts from the total H$_2$ chemisorption measured at RT by using the volumetric method. Also, this method was applied by Yuan and Damiani for characterization of RuMo/SiO$_2$ catalysts [16,17]. More frequently, the bimetallic Ru-Mo catalysts were characterized by the CO chemisorption (pulse or volumetric method) [9,13,15,17].

In this study, chemisorption of hydrogen was performed at RT and 100 °C since our and recently published data have shown that temperature of 100 °C is the most suitable for the volumetric H$_2$ chemisorption on Ru/γ-Al$_2$O$_3$ [21,22,43]. Hydrogen chemisorption data for the all catalysts are summarized in Table 5. Chemisorption of H$_2$ on the 1.6% Mo/γ-Al$_2$O$_3$ catalyst does not occur both at RT and 100 °C. With increasing the Mo loading to 4.8%, a small total H$_2$ adsorption is detected (~10 μmol/g cat.). On the 9.5% Mo/γ-Al$_2$O$_3$ catalyst the H$_2$ uptakes at RT and especially at 100 °C were slightly higher, and even small amount of hydrogen was irreversible chemisorbed (9 μmol/g cat.). XPS analysis of this sample indicated the presence of a small amount of Mo in the metal state (Mo°, Table 3), and it is well-known that dissociative chemisorption of hydrogen occurs on the metallic molybdenum surface [44].

Chemisorption of hydrogen on the Ru and bimetallic Ru-Mo catalysts is significantly higher evidencing that hydrogen is preferably

Table 4

The O$_2$ uptake results for the reduced monometallic Mo, Ru and bimetallic Ru-Mo/γ-Al$_2$O$_3$ catalysts measured at RT and 400 °C.

Catalyst	O$_2$ uptake (μmol/g cat.)		Calculated O$_2$ uptake to oxidation Mo to MoO$_3$ or Ru to RuO$_2$ (μmol/g cat.)	Average oxidation state		
	RT	400 °C		Ru[a]	Mo[a]	Mo[b] (XPS data)
1.6%Mo	4.2	28.3	250	–	Mo$^{5.3}$	Mo$^{5.4}$
4.8%Mo	28.5	103.7	742	–	Mo$^{5.16}$	Mo$^{5.2}$
9.5%Mo	96.1	303.8	1486	–	Mo$^{4.78}$	Mo$^{4.7}$
5%Ru	450.2	571.6	495	Ru^{4+}	–	–
5%Ru-1.6%Mo	481.9	591.6	745	Ru^{4+}	Mo$^{5.00}$	Mo$^{5.1}$
5%Ru-4.8%Mo	529.4	699.6	1237	Ru^{4+}	Mo$^{4.96}$	Mo$^{4.9}$
5%Ru-9.5%Mo	793.5	1548.0	1981	Ru^{4+}	Mo$^{2.06}$	Mo$^{3.74}$

[a] Calculated from the amount of oxygen consumed during oxidation in oxygen at 400 °C of the *in situ* reduced catalysts.

[b] Determined from XPS data.

Table 5

H$_2$ uptakes measured at 20 and 100 °C, dispersion data and the mean size of metal particles for the monometallic (Mo, Ru) and bimetallic Ru–Mo/γ-Al$_2$O$_3$ catalysts.

Catalyst	Temp. (°C)	H$_2$ uptake (μmol/g cat.)			Ruthenium dispersion[a] (H/Ru)	d$_{av}$ (chem)[b] (nm)	d$_{av}$ (TEM) (nm)
		Total	Reversible	Irreversible			
1.6%Mo	20	–	–	–			
	100	–	–	–	–		
4.8%Mo	20	9	9	–			
	100	10	8	2	–		
9.5%Mo	20	12	10	2			
	100	22	13	9	–		
5%Ru[c]	20	150	28	122			
	100	158	30	128	0.52	1.6	1.4 ± 0.6
5%Ru-1.6%Mo	20	162	38	124			
	100	210	75	135	0.55	1.5	1.3 ± 0.5
5%Ru-4.8%Mo	20	62	19	43			
	100	140	40	100	0.41	1.8	1.0 ± 0.4
5%Ru-9.5%Mo	20	24	9	15			
	100	81	21	60	0.24	3.4	0.8 ± 0.1

[a] Number of H atoms irreversible adsorbed at 100 °C to the total number of Ru atoms in the catalyst sample, assuming H/Ru$_s$ = 1.

[b] Average particle size calculated from Ru dispersion measured from H$_2$ adsorption data at 100 °C.

[c] Data from our previous studies [22].
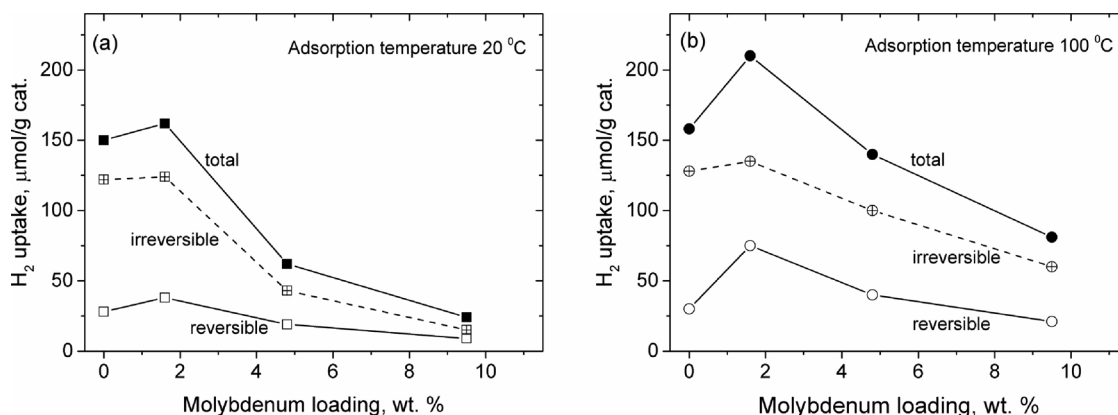
Fig. 8. Effect of molybdenum loading on the hydrogen chemisorption at 20 °C (a) and 100 °C (b) over bimetallic Ru-Mo/γ-Al$_2$O$_3$ catalysts. *Dash lines* represent the irreversibly H$_2$ uptakes.
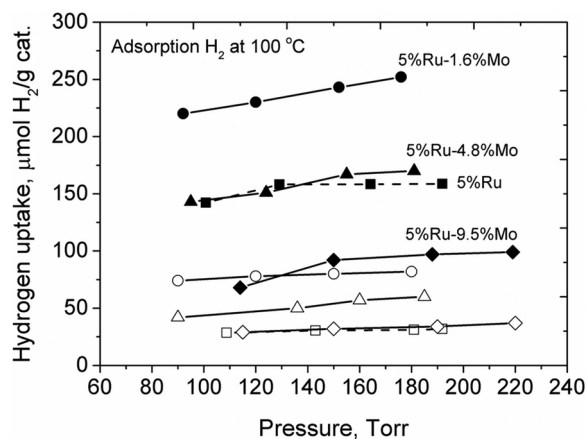
Fig. 9. Typical H$_2$ adsorption isotherms at 100 °C on Ru/γ-Al$_2$O$_3$ (*dash lines*) and on the bimetallic Ru-Mo/γ-Al$_2$O$_3$ catalysts (*solid lines*). *Full* and *empty* symbols represent the total and reversible H$_2$ uptakes, respectively.

adsorbed on the Ru atoms than on the MoO$_x$ species (Table 5). The effect of the Mo loading on hydrogen chemisorption over Ru-Mo catalysts is presented, for clarity, also in Fig. 8. The total H$_2$ uptakes at 100 °C are always higher than these at RT, especially for the bimetallic Ru-Mo catalysts, and the differences are partly due to higher amount of

the reversibly bound hydrogen. Fig. 9 shows typical isotherms of hydrogen chemisorption at 100 °C on the Ru and Ru-Mo catalysts. On the bimetallic 5%Ru-1.6%Mo/γ-Al$_2$O$_3$ catalyst the total H$_2$ uptake at 100 °C (210 μmol/g cat.) is much higher than on monometallic Ru/γ-Al$_2$O$_3$ (158 μmol/g cat.) and Ru-Mo samples containing 4.8% or 9.5% Mo (140 and 81 μmol/g cat., respectively). Therefore, addition of small amount of Mo (Ru:Mo = 3:1) is very favourable for hydrogen chemisorption on the Ru-Mo sample. The difference between the total and reversibly adsorption yields the amount of strongly chemisorbed hydrogen, which after extrapolation to zero pressure, gives the capacity of a hydrogen monolayer (Table 5). For the monometallic Ru catalyst only small differences between the irreversible H$_2$ chemisorption were observed at RT and 100 °C (122 and 128 μmol/g cat., respectively), evidencing that the saturation of the Ru surface with hydrogen is achieved already at RT. Similarly, for the bimetallic sample containing 1.6% Mo (Ru/Mo = 3:1) these differences (124 and 135 μmol/g cat., respectively) are not large, although differences between the total and reversible hydrogen chemisorption were significant. For the samples with Mo loading of 4.8% and 9.5%, irreversible H$_2$ uptakes significantly increase with rise of adsorption temperature (by 2.3 or 4 times, respectively), suggesting an activated adsorption of hydrogen on the bimetallic Ru-Mo catalysts. We suppose that close interaction between Ru and Mo species could induce such adsorption process. Literature data show that adsorption of other atoms or molecules on Ru particles can strongly affect the strength of hydrogen adsorption, through direct electronic interference, causing attractive or repulsive interactions with

co-adsorbed hydrogen [21,43]. Presented work is the first literature report showing activated hydrogen adsorption on the bimetallic Ru-Mo catalysts. Interestingly, the amount of reversibly adsorbed hydrogen (expressed as percentage of the total H_2 uptake) is always higher on the bimetallic Ru-Mo catalysts as compared to the Ru sample. The weakly adsorbed hydrogen may be considered as relatively reactive hydrogen, which may contribute to the synergistic effect observed in the Ru-Mo catalysts [4]. One of the possible explanation for the increase of the reversibly bound hydrogen could be a preferential occupancy of Ru defect sites in small nanoparticles (edges and kinks, that are expected to strongly bind H atoms) by Mo species. Similar interpretation was proposed for hydrogen chemisorption results on the bimetallic Ru-Cu/SiO$_2$ catalysts [45]. HRTEM data evidently show that interaction between Ru and Mo species facilitates formation of smaller particles (1.3 -0.8 nm) as compared to the monometallic Ru catalyst (1.4 nm). Theoretical calculations predicted also a non-uniform distribution of Mo atoms in the outermost atomic layer in Pt$_{80}$Mo$_{20}$ nanoparticles: the Pt atoms occupied preferentially the facet sites, while Mo atoms favour the low co-ordination edge and vertex sites [46].

Since for the bimetallic Ru-Mo catalysts saturation of a hydrogen monolayer corresponding to $H/Ru_s = 1/1$ was not achieved at RT, metal dispersion was calculated from the irreversible H_2 uptake at 100 °C (Table 5). Only for the bimetallic sample with low Mo loading (Ru:Mo = 3:1) the irreversible H_2 uptake was slightly higher (135 μmol/g cat.) than for the monometallic 5% Ru/γ-Al$_2$O$_3$ catalyst (128 μmol/g cat.). However, the irreversible H_2 uptake was decreased to 100 μmol/g cat. and to around 60 μmol/g cat. for the bimetallic catalysts containing 4.8% or 9.5% Mo, respectively (Ru:Mo = 1:1 or 1:2). The continuous trend of decrease in the irreversible H_2 uptake with the Mo loading (see Fig. 10) suggests enlarging coverage of surface Ru metal with MoO$_x$ species, because the number of exposed Ru atoms available for hydrogen chemisorption is reduced. Although, XPS measurements showed a two-fold increase in surface coverage of ruthenium with an increase in Mo loading but surface enrichment by Mo was much higher i.e. ~14 times (Table 3). Another possibility is a modification of the chemisorption properties of ruthenium caused by the formation of Ru-Mo bonds between metallic Ru and Mo. The largest suppression of hydrogen chemisorption was found for the 5%Ru-9.5%Mo catalyst for which XPS analysis indicated the presence of about 25 at% of Mo in the metallic state (Table 3). Although hydrogen adsorbs on Mo in the metallic state (Mo°) [44] however, it is possible that the presence of unreduced molybdenum species leads to weaken the H_2-Mo° interaction or even prevents hydrogen from adsorbing on Mo°. Such a hypothesis was proposed by Leclercq et al. to explain hydrogen chemisorption data on the Pt-Mo/SiO$_2$ catalysts [34]. Decrease of ruthenium dispersion (H/Ru) from 0.52 for the 5% Ru/γ-Al$_2$O$_3$ catalyst to 0.41 or 0.24 for the bimetallic 5%Ru-4.8% Mo (Ru:Mo = 1:1) or 5%Ru-9.5%Mo (Ru:Mo = 1:2) catalysts, respectively, means that about 21 or 54% of surface Ru metal was covered by the MoO$_x$ species. Only, addition of

small amount of Mo to the Ru catalyst (Ru:Mo = 3:1) causes some increase of Ru dispersion (H/Ru = 0.55, Table 5). It can be noted that the effect of Mo in the Ru-Mo/γ-Al$_2$O$_3$ catalysts on the Ru dispersion is different from that found previously for the Re-containing Ru/γ-Al$_2$O$_3$ catalysts. In 2014, based on the H_2 chemisorption and HRTEM, we reported that Re greatly improves the dispersion of Ru metal species (expressed as H/Ru) in the Ru-Re/γ-Al$_2$O$_3$ catalysts [22]. Our chemisorption results agree well with Chen et al. [13] who found that addition of low Mo-content (Mo/Ru = 0.2) to Ru/ZrO$_2$ catalysts results in the increase Ru dispersion (based on pulse CO adsorption), while the presence of high Mo-content produce an important decrease in the Ru dispersion. Very recently Tamura et al. [9] reported significant decrease of CO/Ru value from 0.14 over Ru/SiO$_2$ to 0.04 over Ru-MoO$_x$/SiO$_2$ (Mo/Ru = 1:2) catalyst suggesting that about 70% of the surface Ru metal was covered by MoO$_x$ species. Also, Hakim et al. [8] showed recently large decrease in CO chemisorption for the RhMo/C and PtMo/C catalysts as compared to the Rh/C or Pt/C samples. The authors claimed that the active sites on RhMo and PtMo catalysts consisted of a small ensemble of Rh or Pt atoms adjacent to a highly reduced Mo moiety that is coordinated to the precious metal nanoparticle. When the loading of Mo was increased, higher concentration of Mo species are located at the surface of Rh or Pt nanoparticles forming Mo-Rh or Mo-Pt bonds [8].

Fig. 10 shows the effect of the Mo loading in the bimetallic Ru-Mo/γ-Al$_2$O$_3$ catalysts on the average metal particle sizes measured by TEM and the amount of H_2 chemisorption expressed as H/Ru. The average size of the metal particles decreased monotonically on Ru-Mo/γ-Al$_2$O$_3$ catalysts with molar ratio of $0 \leq Ru:Mo \leq 2$, although the amount of H_2 chemisorption decreases with increasing of Mo in the bimetallic catalysts. Because of this, the mean particle size calculated from adsorption data does not agree with TEM (Table 5). Koso et al. also found for the Rh-MoO$_3$/SiO$_2$ that the amount of CO and H_2 adsorption was smaller than expected from the metallic particles determined from XRD and TEM [6]. The authors suggested that at the range of Mo/Rh ≤ 0.13 the addition of one atom of Mo decreases one molecule of the adsorbed CO and all the added Mo atoms can interact with the surface of Rh metal atoms.

3.7. Catalytic measurements

The bimetallic Ru-Mo catalysts containing 1.6 and 4.8% Mo were investigated in detail for their catalytic activity towards propane combustion, and the conversion curves as a function of reaction temperatures are presented in Fig. 11 (first and second run), and catalytic data, including also those on the monometallic Ru and 5%Ru-9.5%Mo catalyst, are summarized in Table 6. In the first run (Fig. 11A), the monometallic 5% Ru/γ-Al$_2$O$_3$ sample shows 100% conversion and values of the temperatures for conversion of 10%, 50% and 95% (T$_{10}$, T$_{50}$ and T$_{95}$) are 160, 173 and 220 °C (Table 6). Over the bimetallic Ru-Mo
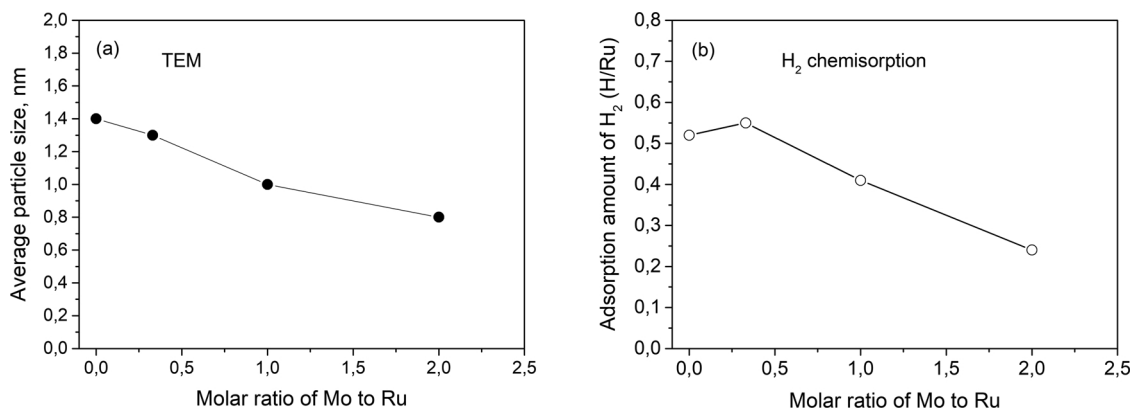

Fig. 10. Effect of additive amount of Mo to 5%Ru/γ-Al$_2$O$_3$ catalyst on the Ru metal particle size determined by HRTEM (a) and the amount of H_2 chemisorption (b).
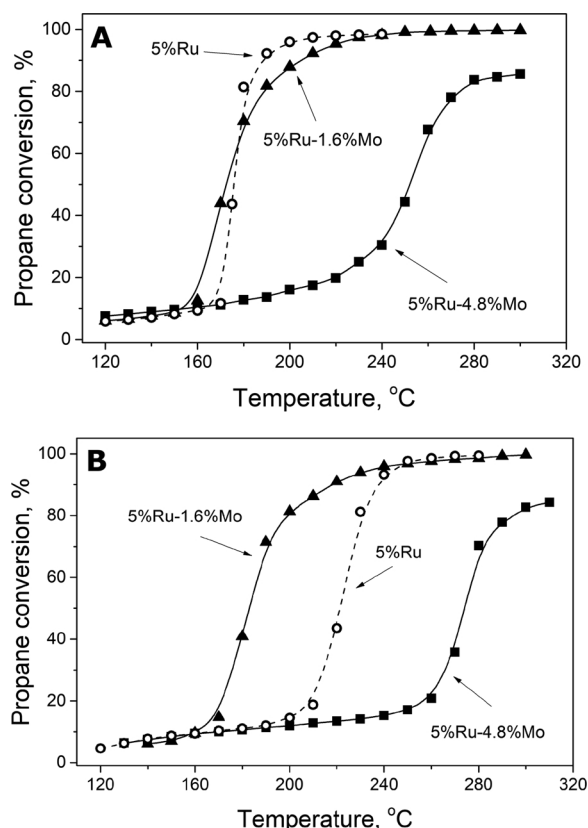
Fig. 11. Propane conversion as a function of temperature over the reduced monometallic Ru/γ-Al$_2$O$_3$ (*open symbols*) and over bimetallic Ru-Mo catalysts containing 1.6 and 4.8% Mo (*full symbols*). The first test (A) and the second test (B). *Experimental conditions*: propane concentration: 800 vppm in air, total flow rate: 100 cm^3 min^{-1}: mass of the catalyst: 100 mg, pressure: atmospheric.

catalysts containing the same amount of Ru (5 wt.%) propane conversion greatly depends on the composition and the conversion curves shift towards higher temperature when the Mo content rise from 1.6 to 4.8 wt.% (Fig. 11A). For the most active 5%Ru-1.6%Mo catalyst, the light of temperature is about 88 °C lower (T$_{50}$ = 170 °C) than that for the 5%Ru-4.8%Mo catalyst (T$_{50}$ = 258 °C). In addition, a bimetallic catalyst containing 4.8 wt.% Mo (Ru:Mo = 1:1) does not achieve 100% conversion of propane in the tested temperature range. Moreover, as shown in Table 6, bimetallic catalyst containing 9.5% Mo (Ru:Mo = 1:2) does not reach even 50% propane conversion in the studied temperature range (120–320 °C). For this catalyst the temperature for conversion of 10% amount to 235 °C and it is much higher than for other samples tested (Table 6). At a maximum reaction temperature of 320 °C, this catalyst has a propane conversion of 30%. Since activity of this catalyst was low only one catalytic test was performed. Furthermore, T$_{10}$, T$_{50}$ and T$_{95}$ values included in Table 6 evidently indicated that only bimetallic catalyst containing 1.6% Mo (Ru:Mo = 3:1) shows

better light–off characteristic than the monometallic Ru sample. The temperature at which 95% conversion is reached is 20 °C lower for the bimetallic 5%Ru-1.6%Mo catalyst (T$_{95}$ = 200 °C) than for the Ru sample (T$_{95}$ = 220 °C).

In the second run, for the most active bimetallic 5%Ru-1.6%Mo catalyst T$_{50}$ value (T$_{50}$ = 180 °C) was only 10 °C higher than in the first run, indicating that no significant catalyst deactivation takes place under oxygen-rich reaction conditions (Table 6). Similar stability exhibited the less active catalyst with the higher Mo content (Fig. 11B). Opposite, for the monometallic Ru catalyst, the T$_{50}$ value was about 48 °C higher as compared to the bimetallic sample containing 1.6% Mo (Table 6), what indicates that large decrease in the amount of exposed Ru surface take place during consecutive runs of propane oxidation.. Probably structural changes of the monometallic Ru catalyst during the course of the propane combustion are greater than that on the bimetallic samples. The superior catalytic performance of the bimetallic Ru-Mo catalyst with the Mo loading of 1.6 wt.% is not the result of the additive effect of molybdenum and ruthenium because the monometallic Mo/γ-Al$_2$O$_3$ samples at each loading were completely inactive in the propane combustion in the studied temperature range (120–320 °C). We assume that the differences in conversion curves of Fig. 11 should be partly explained by the variation in the amount of the exposed active ruthenium surface since ruthenium dispersion was enhanced when the small amount of molybdenum (Ru:Mo = 3:1) was added to the Ru/γ-Al$_2$O$_3$ catalyst (Table 5). The improvement of the catalytic performance may also be explained by favorable Ru-Mo interactions because, as found by XPS, the amount of easily oxidizable Ru sites, which are active for propane combustion [11,20,37], is higher for the 5%Ru-1.6%Mo catalyst (81.2%) than for the Ru sample (72%) and bimetallic samples with higher Mo loading (47.8 or 26.2% for 4.8% Mo or 9.5% Mo, respectively, Table 3). In previous papers we showed that the partly oxidized RuO$_x$ species or amorphous RuO$_2$ particles are the catalytically active phases in propane combustion [11,20,37]. Since according to the literature data, it is believed that the Mars-van-Krevelen (redox) mechanism plays a role in the VOCs oxidation on the supported Ru catalysts, it is reasonable to assume that propane oxidation over the bimetallic Ru-Mo/γ-Al$_2$O$_3$ catalysts also proceed *via* this mechanism. The better stability of bimetallic Ru-Mo catalysts may be also connected with the synergic effect between Ru and Mo. A similar promotion effect of molybdenum and tungsten was found when Pt/Al$_2$O$_3$ catalyst was applied for propane and methane combustion [47,48]. We recently also reported that Ru-Re/γ-Al$_2$O$_3$ catalysts (Re loading ≤ 3 wt.%) were more active and stable in the propane combustion than the Ru catalyst [11]. Addition of Re improved also catalytic activity of the Ru/γ-Al$_2$O$_3$ catalysts for the methane combustion but thermal stability of the bimetallic Ru-Re catalysts for this reaction was similar to that of the monometallic Ru catalyst [12].

Results of kinetic measurements obtained under differential reaction conditions are summarized in the Arrhenius plots of Fig. 12. The TOF values were calculated from the propane oxidation rate expressed in micromoles of propane converted on 1 g of the catalyst per second (μmol g$_{cat}^{-1}$ s^{-1}) and the active site concentration determined from H$_2$ chemisorption results (μmol/g cat.). It is seen that the specific reaction

Table 6
Comparison of the catalytic properties of ruthenium for propane oxidation over reduced monometallic Ru/γ-Al$_2$O$_3$ and bimetallic Ru-Mo/γ-Al$_2$O$_3$ catalysts.

Catalyst	Catalytic activity in terms of conversion temperature (°C)			Specific reaction rate [a] (μmol/ g^{-1} s^{-1})	TOF (s^{-1}) 1.0 ± 0.4	E$_{app}$ (kcal/mol)
	T$_{10}$	T$_{50}$	T$_{95}$			
5% Ru/γ-Al$_2$O$_3$	160	173/221	220	0.74	2.9 × 10^{-3}	20.2
5% Ru-1.6%Mo/γ-Al$_2$O$_3$	155	170/180	200	0.93	3.4 × 10^{-3}	20.7
5% Ru-4.8%Mo/γ-Al$_2$O$_3$	160	258/273	n.d[b]	0.33	1.6 × 10^{-3}	17.7
5% Ru-9.5%Mo/γ-Al$_2$O$_3$	235	n.d. [b]	n.d. [b]	–	–	–

[a] Specific reaction rate and TOF calculated at 165 °C.
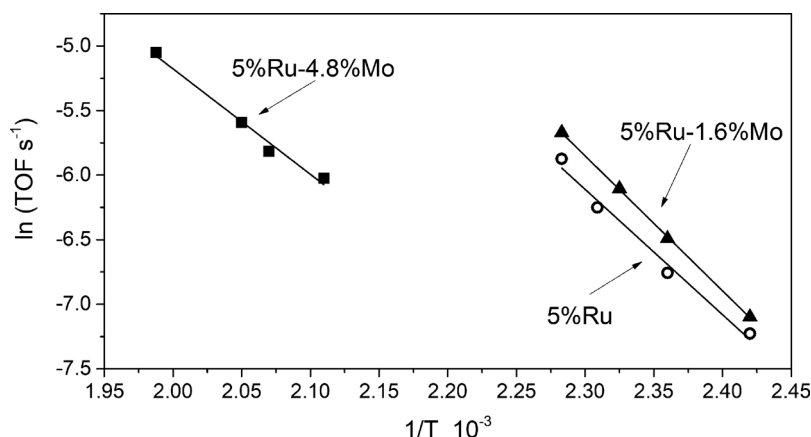[b] In the tested temperature range (120–320 °C) the catalyst sample does not reach 50 or 95% propane conversion.

Fig. 12. Arrhenius-type plots for propane combustion of the monometallic Ru (*open symbols*) and bimetallic Ru-Mo catalysts containing 1.6 and 4.8% Mo (*full symbols*).

rate (TOF) greatly depend on the Mo loading in the bimetallic samples and the 5%Ru-4.8%Mo catalyst is much less active than that containing 1.6%Mo. The most active 5%Ru-1.6%Mo catalyst possesses the specific reaction rate slightly higher than the monometallic 5%Ru catalyst. The apparent activation energy E_{app} for the most active 5%Ru-1.6%Mo catalyst (20.7 kcal/mol) is similar to that found over the 5%Ru catalyst (20.2 kcal/mol) but it is somewhat lower for the less active 5%Ru-4.8% Mo catalyst (17.7 kcal/mol). We suppose that higher concentration of Mo in close contact with surface ruthenium species may slightly facilitate activation of C–H bond in propane. From the density functional theory studies it was found that MoO_3 supported Pt catalysts can also facilitate single C–H bond activation in methane [49]. On the other hand, in the 5%Ru-4.8%Mo sample part of ruthenium phase is unavailable for reaction, which causes its lower catalytic performance. The values of the specific reaction rates expressed in $\mu mol\ CH_3H_8$ reacted per g_{cat} and per second and the TOFs (s^{-1}), measured at low reaction temperature of 165 °C (kinetic region), are presented in Table 6. It is clearly visible that 5%Ru-1.6%Mo catalyst shows about 25% higher reaction rate of propane oxidation as compared to the monometallic Ru sample. However, bimetallic Ru-Mo catalyst with Mo loading of 4.8% shows about three times lower reaction rate as compared to the sample with the low Mo content. Also, as shown in the Table 6, the TOF calculated at 165 °C for the most active 5%Ru-1.6%Mo catalyst (with dispersion H/Ru = 0.55) is about two times higher as compared to the bimetallic sample with 4.8% Mo (with dispersion H/Ru = 0.41). It could be noted that Ru-based catalysts, for which activity data are presented, have identical Ru content (5 wt.%), as well as very small and similar mean particle size (1.4-1.0 nm, Fig. 5), hence one of the possible factors affecting the catalyst activity could be associated with some blocking of the active Ru sites by the inactive MoO_x species. The blocking effect was particularly large for the bimetallic Ru-Mo catalyst containing of 9.5% Mo, for which activity was very low (Table 6). The activity results are in full agreement with XPS and H_2 and O_2 chemisorption data, which evidence that Ru active phase is partly covered by oxidized molybdenum species what cause lowering catalytic activity of the bimetallic Ru-Mo catalyst with higher Mo loading ($\geq$ 4.8 wt.% Mo) at low temperatures. Also, as shown in Fig. 11a, at higher reaction temperatures (200–320 °C), the bimetallic catalyst with the atomic ratio Ru:Mo = 1:1 gave poorer catalytic performance than the sample with atomic ratio of 3:1. Similarly, the literature data indicates that Ru/Mo systems, applied for the reaction of hydrocarbons with hydrogen, are prone to deactivation at higher Ru:Mo atomic ratio due to blocking of metallic active sites by molybdenum oxides species [10,33]. Beamson et al. reported that for the unsupported Ru/Mo catalysts, depending on the Mo:Ru atomic ratio, synergistic or poisoning effects were observed for the selective hydrogenation of amides, with the optimum combination for conversion and

selectivity at ˜0.5, and the complete inhibition of catalysis at Mo:Ru $\geq$ 1 [10].

4. Conclusion

A series of bimetallic Ru-Mo/γ-Al$_2$O$_3$ catalysts with the Ru/Mo atomic ratio of 3:1, 1:1 and 1:2 was prepared by the co-impregnation method and tested in the propane oxidation for the first time. The addition of small amount of molybdenum (1.6%) improved the catalytic performance (activity and stability) of the bimetallic Ru-Mo catalyst. At the higher Mo content (Ru:Mo atomic ratio of 1:1 and 1:2) a suppress of activity caused by the blocking of the active ruthenium phase by MoO_x species was observed. The enhanced activity was explained by higher dispersion of ruthenium in the 5%Ru-1.6%Mo catalyst as compared to the monometallic 5%Ru and high loaded bimetallic samples. The synergy effect observed especially over the bimetallic Ru-Mo catalyst at Ru:Mo atomic ratio of 3:1 for oxidation of propane may also correspond to the redox interaction between Mo and Ru species. XPS data clearly show that the ruthenium oxidation state was affected by the presence of Mo. The interaction of highly dispersed partly oxidized RuO_x species with the alumina support is stronger when the molybdenum was added what enhance resistance of bimetallic Ru-Mo catalysts to deactivation under oxygen-rich reaction conditions. Favorable changes in the chemisorption properties of ruthenium were also observed, such as weakening of the hydrogen bonding force and the activated nature of the adsorption process in the bimetallic Ru-Mo catalysts.

Appendix A. Supplementary data

Supplementary material related to this article can be found, in the online version, at doi:https://doi.org/10.1016/j.apcatb.2019.01.059.

References

[1] T.V. Choudhary, S. Banerjee, V.R. Choudhary, Catalysts for combustion of methane and lower alkanes, Appl. Catal. A Gen. 234 (2002) 1–23, https://doi.org/10.1016/S0926-860X(02)00231-4.

[2] Z. Zhu, G. Lu, Y. Guo, Y. Guo, Z. Zhang, Y. Wang, X.-Q. Gong, High performance and stability of the Pt-W/ZSM-5 catalyst for the total oxidation of propane: the role of

tungsten, ChemCatChem 5 (2013) 2495–2503, https://doi.org/10.1002/cctc.201300101.

[3] J. Chen, H. Arandiyan, X. Gao, J. Li, Recent advances in catalysts for methane combustion, Catal. Surv. Asia 19 (2015) 140–171, https://doi.org/10.1007/s10563-015-9191-5.

[4] K. Tomishige, Y. Nakagawa, M. Tamura, Selective hydrogenolysis and hydrogenation using metal catalysts directly modified with metal oxide species, Green Chem. 19 (2017) 2876–2924, https://doi.org/10.1039/C7GC00620A.

[5] D. Ballesteros-Plata, A. Infantes-Molina, M. Rodríguez-Cuadrado, E. Rodríguez-Aguado, P. Braos-García, E. Rodríguez-Castellón, Incorporation of molybdenum into Pd and Pt catalysts supported on commercial silica for hydrodeoxygenation reaction of dibenzofuran, Appl. Catal. A Gen. 547 (2017) 86–95, https://doi.org/10.1016/J.APCATA.2017.08.034.

[6] S. Koso, H. Watanabe, K. Okumura, Y. Nakagawa, K. Tomishige, Comparative study of Rh–MoOx and Rh–ReOx supported on SiO2 for the hydrogenolysis of ethers and polyols, Appl. Catal. B Environ. 111–112 (2012) 27–37, https://doi.org/10.1016/J.APCATB.2011.09.015.

[7] M. Chia, B.J. O'Neill, R. Alamillo, P.J. Dietrich, F.H. Ribeiro, J.T. Miller, J.A. Dumesic, Bimetallic RhRe/C catalysts for the production of biomass-derived chemicals, J. Catal. 308 (2013) 226–236, https://doi.org/10.1016/J.JCAT.2013.08.008.

[8] S.H. Hakim, C. Sener, A.C. Alba-Rubio, T.M. Gostanian, B.J. O'Neill, F.H. Ribeiro, J.T. Miller, J.A. Dumesic, Synthesis of supported bimetallic nanoparticles with controlled size and composition distributions for active site elucidation, J. Catal. 328 (2015) 75–90, https://doi.org/10.1016/J.JCAT.2014.12.015.

[9] M. Tamura, N. Yuasa, Y. Nakagawa, K. Tomishige, Selective hydrogenation of nitroarenes to aminoarenes using a MoOx -modified Ru/SiO2 catalyst under mild conditions, Chem. Commun. 53 (2017) 3377–3380, https://doi.org/10.1039/C7CC00653E.

[10] G. Beamson, A.J. Papworth, C. Philipps, A.M. Smith, R. Whyman, Selective hydrogenation of amides using ruthenium/molybdenum catalysts, Adv. Synth. Catal. 352 (2010) 869–883, https://doi.org/10.1002/adsc.200900824.

[11] K. Baranowska, J. Okal, Bimetallic Ru-Re/γ-Al2O3 catalysts for the catalytic combustion of propane: effect of the Re addition, Appl. Catal. A Gen. 499 (2015) 158–167, https://doi.org/10.1016/J.APCATA.2015.04.023.

[12] J. Okal, M. Zawadzki, K. Baranowska, Methane combustion over bimetallic Ru-Re/γ-Al2O3 catalysts: effect of Re and pretreatments, Appl. Catal. B Environ. 194 (2016) 22–31, https://doi.org/10.1016/J.APCATB.2016.04.038.

[13] L. Chen, Y. Zhu, H. Zheng, C. Zhang, Y. Li, Aqueous-phase hydrodeoxygenation of propanoic acid over the Ru/ZrO2 and Ru–Mo/ZrO2 catalysts, Appl. Catal. A Gen. 411–412 (2012) 95–104, https://doi.org/10.1016/J.APCATA.2011.10.026.

[14] C.E. Scott, P. Betancourt, M.J. Pérez Zurita, C. Bolívar, J. Goldwasser, A study of Ru-Mo/Al2O3 catalysts, Appl. Catal. A Gen. 197 (2000) 23–29, https://doi.org/10.1016/S0926-860X(99)00529-3.

[15] C.E. Scott, T. Romero, E. Lepore, M. Arruebarrena, P. Betancourt, C. Bolívar, M.J. Pérez-Zurita, P. Marcano, J. Goldwasser, Interaction between ruthenium and molybdenum in RuMo/Al2O3 catalysts, Appl. Catal. A Gen. 125 (1995) 71–79, https://doi.org/10.1016/0926-860X(94)00270-3.

[16] A. Juan, D.E. Damiani, Supported Ru-Mo catalysts for syngas reaction to oxygenates, J. Catal. 137 (1992) 77–91, https://doi.org/10.1016/0021-9517(92)90140-D.

[17] A. Juan, D.E. Damiani, Characterization of RuMo–SiO2 catalysts. A comparative study before and after CO hydrogenation reaction, J. Mater. Chem. 6 (1996) 1433–1439, https://doi.org/10.1039/JM9960601433.

[18] Y. Yang, Q. Liu, D. Li, J. Tan, Q. Zhang, C. Wang, L. Ma, Selective hydrodeoxygenation of 5-hydroxymethylfurfural to 2,5-dimethylfuran on Ru–MoOx /C catalysts, RSC Adv. 7 (2017) 16311–16318, https://doi.org/10.1039/C7RA00605E.

[19] P. Reyes, M.E. König, G. Pecchi, I. Concha, M. López Granados, J.L.G. Fierro, o-Xylene hydrogenation on supported ruthenium catalysts, Catal. Lett. 46 (1997) 71–75, https://doi.org/10.1023/A:1019002114936.

[20] J. Okal, M. Zawadzki, Influence of catalyst pretreatments on propane oxidation over Ru/γ-Al2O3, Catal. Lett. 132 (2009) 225–234, https://doi.org/10.1007/s10562-009-0100-2.

[21] J. Okal, M. Zawadzki, L. Kępiński, L. Krajczyk, W. Tylus, The use of hydrogen chemisorption for the determination of Ru dispersion in Ru/γ-alumina catalysts, Appl. Catal. A Gen. 319 (2007) 202–209, https://doi.org/10.1016/J.APCATA.2006.12.005.

[22] K. Baranowska, J. Okal, N. Miniajluk, Effect of rhenium on ruthenium dispersion in the Ru–Re/γ-Al2O3 catalysts, Catal. Lett. 144 (2014) 447–459, https://doi.org/10.1007/s10562-013-1169-1.

[23] I.E. Wachs, Raman and IR studies of surface metal oxide species on oxide supports: supported metal oxide catalysts, Catal. Today 27 (1996) 437–455, https://doi.org/10.1016/0920-5861(95)00203-0.

[24] R. López Cordero, A. López Agudo, Effect of water extraction on the surface properties of Mo/Al2O3 and NiMo/Al2O3 hydrotreating catalysts, Appl. Catal. A Gen. 202 (2000) 23–35, https://doi.org/10.1016/S0926-860X(00)00449-X.

[25] G. Tsilomelekis, S. Boghosian, On the configuration, molecular structure and vibrational properties of MoOx sites on alumina, zirconia, titania and silica, Catal. Sci. Technol. 3 (2013) 1869, https://doi.org/10.1039/c3cy00057e.

[26] D.O. Scanlon, G.W. Watson, D.J. Payne, G.R. Atkinson, R.G. Egdell, D.S.L. Law, Theoretical and experimental study of the electronic structures of MoO3 and MoO2, J. Phys. Chem. C 114 (2010) 4636–4645, https://doi.org/10.1021/jp9093172.

[27] J. Baltrusaitis, B. Mendoza-Sanchez, V. Fernandez, R. Veenstra, N. Dukstiene, A. Roberts, N. Fairley, Generalized molybdenum oxide surface chemical state XPS determination via informed amorphous sample model, Appl. Surf. Sci. 326 (2015) 151–161, https://doi.org/10.1016/J.APSUSC.2014.11.077.

[28] Y.V. Plyuto, I.V. Babich, I.V. Plyuto, A.D. Van Langeveld, J.A. Moulijn, XPS studies of MoO3/Al2O3 and MoO3/SiO2 systems, Appl. Surf. Sci. 119 (1997) 11–18, https://doi.org/10.1016/S0169-4332(97)00185-2.

[29] J.-G. Choi, L.T. Thompson, XPS study of as-prepared and reduced molybdenum oxides, Appl. Surf. Sci. 93 (1996) 143–149, https://doi.org/10.1016/0169-4332(95)00317-7.

[30] M. Langpape, J.M.M. Millet, U.S. Ozkan, P. Delichère, Study of cesium or cesium–transition metal-substituted keggin-type phosphomolybdic acid as isobutane oxidation catalysts: II. Redox and catalytic properties, J. Catal. 182 (1999) 148–155, https://doi.org/10.1006/JCAT.1998.2359.

[31] B.V. Crist, Handbooks of Monochromatic XPS Spectra Volume 2 - Commercially Pure Binary Oxides, XPS Int. LCC, 2005, http://www.xpsdata.com.

[32] Y.L. Leung, P.C. Wong, K.A.R. Mitchell, K.J. Smith, X-ray photoelectron spectroscopy studies of the reduction of MoO3 thin films by NH3, Appl. Surf. Sci. 136 (1998) 147–158, https://doi.org/10.1016/S0169-4332(98)00341-9.

[33] N. Boufaden, R. Akkari, B. Pawelec, J.L.G. Fierro, M.S. Zina, A. Ghorbel, Dehydrogenation of methylcyclohexane to toluene over partially reduced silica-supported Pt-Mo catalysts, J. Mol. Catal. A Chem. 420 (2016) 96–106, https://doi.org/10.1016/J.MOLCATA.2016.04.011.

[34] G. Leclercq, S. Pietrzyk, T. Romero, A. El Gharbi, L. Gengembre, J. Grimblot, F. Aïssi, M. Guelton, A. Latef, L. Leclercq, Investigation on active sites in Pt − Mo on silica catalysts for reactions of hydrocarbons with hydrogen, Ind. Eng. Chem. Res. 36 (1997) 4015–4027, https://doi.org/10.1021/ie9606303.

[35] A. Katrib, J.W. Sobczak, M. Krawczyk, L. Zommer, A. Benadda, A. Jablonski, G. Maire, Surface studies and catalytic properties of the bifunctional bulk MoO2 system, Surf. Interface Anal. 34 (2002) 225–229, https://doi.org/10.1002/sia.1288.

[36] L.E. Briand, O.P. Tkachenko, M. Guraya, I.E. Wachs, W. Grünert, Methodical aspects in the surface analysis of supported molybdena catalysts, Surf. Interface Anal. 36 (2004) 238–245, https://doi.org/10.1002/sia.1679.

[37] J. Okal, M. Zawadzki, W. Tylus, Microstructure characterization and propane oxidation over supported Ru nanoparticles synthesized by the microwave-polyol method, Appl. Catal. B Environ. 101 (2011) 548–559, https://doi.org/10.1016/J.APCATB.2010.10.028.

[38] K. Baranowska, J. Okal, W. Tylus, Microwave-assisted polyol synthesis of bimetallic RuRe nanoparticles stabilized by PVP or oxide supports (γ-alumina and silica), Appl. Catal. A Gen. 511 (2016) 117–130, https://doi.org/10.1016/J.APCATA.2015.11.045.

[39] D.J. Morgan, Resolving ruthenium: XPS studies of common ruthenium materials, Surf. Interface Anal. 47 (2015) 1072–1079, https://doi.org/10.1002/sia.5852.

[40] S. Tougard, QUASES, Software for IMFP Calculation Using TPP2 M Formula, (2010).

[41] A.N. Desikan, L. Huang, S.T. Oyama, Structure and dispersion of molybdenum oxide supported on alumina and titania, J. Chem. Soc. Faraday Trans. 88 (1992) 3357, https://doi.org/10.1039/ft9928803357.

[42] Y.D. Kim, A.P. Seitsonen, S. Wendt, J. Wang, C. Fan, K. Jacobi, H. Over, G. Ertl, Characterization of various oxygen species on an oxide surface: RuO2(110), J. Phys. Chem. B 105 (2001) 3752–3758, https://doi.org/10.1021/JP003213J.

[43] C. Fernández, N. Bion, E.M. Gaigneaux, D. Duprez, P. Ruiz, Kinetics of hydrogen adsorption and mobility on Ru nanoparticles supported on alumina: effects on the catalytic mechanism of ammonia synthesis, J. Catal. 344 (2016) 16–28, https://doi.org/10.1016/J.JCAT.2016.09.013.

[44] T. Wang, X. Tian, Y. Yang, Y.-W. Li, J. Wang, M. Beller, H. Jiao, Structures of seven molybdenum surfaces and their coverage dependent hydrogen adsorption, Phys. Chem. Chem. Phys. 18 (2016) 6005–6012, https://doi.org/10.1039/C5CP07349A.

[45] A.G. Shastri, J. Schwank, S. Galvagno, The microstructure of bimetallic Ru-CuSiO2 catalysts: a chemisorption and analytical electron microscopy study, J. Catal. 100 (1986) 446–457, https://doi.org/10.1016/0021-9517(86)90111-9.

[46] G. Wang, M.A. Van Hove, P.N. Ross, M.I. Baskes, Quantitative prediction of surface segregation in bimetallic Pt–M alloy nanoparticles (M = Ni, Re, Mo), Prog. Surf. Sci. 79 (2005) 28–45, https://doi.org/10.1016/J.PROGSURF.2005.09.003.

[47] Y. Yazawa, H. Yoshida, S. Komai, T. Hattori, The additive effect on propane combustion over platinum catalyst: control of the oxidation-resistance of platinum by the electronegativity of additives, Appl. Catal. A Gen. 233 (2002) 113–124, https://doi.org/10.1016/S0926-860X(02)00129-1.

[48] M. O'Connell, G. Kolb, R. Zapf, Y. Men, V. Hessel, Bimetallic catalysts for the catalytic combustion of methane using microreactor technology, Catal. Today 144 (2009) 306–311, https://doi.org/10.1016/J.CATTOD.2008.10.053.

[49] C.J. Zhang, P. Hu, The possibility of single C–H bond activation in CH4 on a MoO3-supported Pt catalyst: a density functional theory study, J. Chem. Phys. 116 (2002) 4281–4285, https://doi.org/10.1063/1.1449942.